Water-Catalyzed O−H Insertion/HI Elimination Reactions of Isodihalomethanes (CH_2X-I, Where X = Cl, Br, I) with Water and the Dehalogenation of Dihalomethanes in Water-Solvated Environments

Xufeng Lin, Xiangguo Guan, Wai Ming Kwok, Cunyuan Zhao, Yong Du, Yun-Liang Li, and David Lee Phillips*

Department of Chemistry, The University of Hong Kong, Pokfulam Road, Hong Kong S.A.R., P. R. China

Received: October 28, 2004; In Final Form: November 26, 2004

A combined experimental and theoretical investigation of the ultraviolet photolysis of CH_2XI (where X = Cl, Br, I) dihalomethanes in water is presented. Ultraviolet photolysis of low concentrations of CH_2XI (where X = Cl, Br, I) in water appears to lead to almost complete conversion into $CH_2(OH)_2$ and HX and HI products. Picosecond time-resolved resonance Raman (ps-TR^3) spectroscopy experiments revealed that noticeable amounts of CH_2X-I isodihalomethane intermediates were formed within several picoseconds after photolysis of the CH_2XI parent compound in mixed aqueous solutions. The ps-TR^3 experiments in mixed aqueous solutions revealed that the decay of the CH_2X-I isodihalomethane intermediates become significantly shorter as the water concentration increases, indicating that the CH_2X-I intermediates may be reacting with water. Ab initio calculations found that the CH_2X-I intermediates are able to react relatively easily with water via a water-catalyzed O−H insertion/HI elimination reaction to produce $CH_2X(OH)$ and HI products, with the barrier for these reactions increasing as X changes from Cl to Br to I. The ab initio calculations also found that the $CH_2X(OH)$ product can undergo a water-catalyzed HX elimination reaction to make $H_2C{=}O$ and HX products, with the barrier to reaction decreasing as X changes from Cl to Br to I. The preceding two water-catalyzed reactions produce the HI and HX leaving groups observed experimentally, and the $H_2C{=}O$ product further reacts with water to make the other $CH_2(OH)_2$ product observed in the photochemistry experiments. This suggests that that the CH_2X-I intermediates react with water to form the $CH_2(OH)_2$ and HI and HX products observed in the photochemistry experiments. Ultraviolet photolysis of CH_2XI (where X = Cl, Br, I) at low concentrations in water-solvated environments appears to lead to efficient dehalogenation and release of two strong acid leaving groups. We very briefly discuss the potential influence of this photochemistry in water on the decomposition of polyhalomethanes and halomethanols in aqueous environments.

Introduction

A number of polyhalomethanes such as CH_2I_2, CH_2BrI, $CHBr_3$, CCl_4, $CFCl_3$, and others have been observed in the atmosphere and are important sources of reactive halogens in the natural environment.[1−8] The formation of IO during localized ozone-depletion events in the marine boundary layer of the troposphere has been linked to the photochemistry of CH_2I_2 and CH_2BrI.[7,8] The formation of iodine aerosols has also been linked to the photochemistry of CH_2I_2.[9] It is recognized that both gas- and condensed-phase chemistry and photochemistry are needed in accurately describing chemical reaction processes in the natural environment.[9−21] There has been increasing interest in reactions relevant to the activation of halogens in aqueous sea-salt particles.[10−21]

In the gas phase, ultraviolet photolysis of polyhalomethanes typically leads to a direct carbon−halogen bond cleavage to form halomethyl and halogen atom fragments.[22−38] These photofragments can undergo solvent-induced geminate recombination in the condensed phase to form appreciable amounts of isopolyhalomethanes.[39−55] We have elucidated the chemical reactivity of isopolyhalomethanes toward olefins both experimentally and theoretically and observed that they are carbenoid species that can react with C=C bonds in olefins to make cyclopropanated products and a halogen molecule leaving group.[56−61] The results for isodiiodomethane suggested that it is likely the predominant carbenoid responsible for the cyclopropanation of olefins when using the ultraviolet photolysis of CH_2I_2 method, and a reaction mechanism was proposed.[56,58,61] Solvent effects on the isodiiodomethane reaction with olefins have also been recently examined by another group.[62] Other isopolyhalomethanes were found to also undergo similar reactions with the C=C bonds of olefins.[51,57,60]

Carbenoids (as well as carbenes such as singlet methylene and dichlorocarbene) are also able to react with the O−H bonds of water and alcohols via O−H insertion reactions.[63−72] We recently used picosecond time-resolved resonance Raman (ps-TR^3) experiments to directly observe the reaction of isobromoform with water to form a $CHBr_2OH$ product species.[73,74] This indicates isopolyhalomethanes can also react with the O−H bonds of water via O−H insertion reactions such as other carbenoids and carbenes such as singlet methylene and dichlorocarbene. We have also recently investigated a dihalomethane and observed that ultraviolet photolysis of low concentrations of CH_2I_2 in water led to almost complete conversion into $CH_2(OH)_2$ and 2HI products.[75] The ps-TR^3

* Author to whom correspondence should be addressed. Phone: 852-2859-2160. Fax: 852-2857-1586. E-mail: phillips@hkucc.hku.hk.

10.1021/jp0450843 CCC: $30.25
Published on Web 01/27/2005

spectra in mixed aqueous solvents showed that appreciable amounts of isodiiodomethane (CH_2I-I) were formed within several picoseconds and its decay was substantially faster with increasing water concentration.[75] This suggests that the CH_2I-I species may be reacting with water. Ab initio calculations found that CH_2I-I can react with water via a water-catalyzed O−H insertion/HI elimination reaction followed by its $CH_2I(OH)$ product decomposing via a water-catalyzed HI elimination reaction to form a formaldehyde product that then reacts with water to form the methanediol ($CH_2(OH)_2$) product observed in the photochemistry experiments.[75]

In this article, we examine the photochemistry of a series of dihalomethanes (CH_2I_2, CH_2BrI, and CH_2ClI) in water-solvated environments (e.g., pure water and/or water/acetonitrile solvents). We note that all three of these dihalomethanes have been observed in the marine boundary layer of the troposphere.[7] Photochemistry experiments found that ultraviolet photolysis of low concentrations of all three molecules in water led to formation of $CH_2(OH)_2$, as was found previously for the photolysis of CH_2I_2.[75] In addition, HI and HX leaving groups were also produced. These results indicate that the water-catalyzed dehalogenation reactions of isodihalomethanes are likely a common phenomena for a range of dihalomethanes in water-solvated environments. Picosecond time-resolved resonance Raman spectroscopy experiments and ab initio calculations were done to investigate how the water-catalyzed dehalogenation reactions of CH_2X-I isodihalomethanes vary as X changes from Cl to Br to I. We compare how changing X from Cl to Br to I affects the photochemistry of CH_2XI and the water-catalyzed reaction steps and also very briefly discuss the potential influence of this photochemistry in water on the decomposition of polyhalomethanes and halomethanols in aqueous environments.

Experimental and Computational Methods

Photochemistry Experiments. Commercially available CH_2I_2 (99%), $^{13}CH_2I_2$, CH_2BrI, CH_2ClI, formaldehyde in water (reagent grade), D_2O (99.9% D), and deionized water were used to prepare samples for use in the photochemistry and time-resolved Raman experiments. Samples of the dihalomethanes were prepared with concentrations of about 1×10^{-4} M and put into a 10-cm path length glass holder with quartz windows for the photochemistry experiments. The dihalomethane sample solution was excited by an unfocused 266-nm laser beam (~3 mJ) from the fourth harmonic of a Nd:YAG laser in the laser photolysis experiments. The absorption spectra for the photolyzed samples were acquired using a 1 cm UV grade cell and a Perkin-Elmer Lambda 19 UV/vis spectrometer. The pH values of the photolyzed samples were monitored using an THERMO Orion 420A pH meter utilizing a 8102BN combination pH electrode that was calibrated with pH 7.00 and 4.01 standard buffer solutions. ^{13}C and/or ^{1}H NMR spectra were acquired using a Bruker Advance 400 DPX spectrometer and $\phi = 5$-mm sample tubes at room temperature. IR spectra were obtained using a Bio-rad FTS 165 spectrometer utilizing an ~20-μm sample thickness and CaF_2 windows for the sample holder. Spectra were acquired for the sample in H_2O, the H_2O solvent, and a baseline background. The H_2O solvent spectrum and the baseline background spectrum were subtracted from the sample in H_2O spectrum so as to find the resulting sample spectrum.

Picosecond Time-Resolved Resonance Raman Experiments. The experimental apparatus and methods employed for the ps-TR^3 experiments have been described elsewhere, and therefore only a brief description will be given here.[73−75] A commercial picosecond mode-locked Ti:Sapphire regenerative amplifier laser system was utilized in the experiments. The laser output (800 nm, 1 ps, 1 kHz) was frequency doubled and tripled to generate the 400-nm probe and 267-nm pump excitation wavelengths employed in the experiments. Fluorescence depletion of trans-stilbene was employed to find the time-zero delay between the pump and probe laser beams by varying the optical delay between the pump and probe beams to a point were the depletion of the stilbene fluorescence was midway to the maximum fluorescence depletion by the probe laser. The time-zero value found this way was estimated to be accurate to ±0.5 ps with a typical cross correlation time of ~1.5 ps (fwhm). Magic angle polarization was used for the pump and probe laser beams that were lightly focused onto about a 500-μm-thick flowing liquid stream of sample. Typical pulse energies and spot sizes at the sample were 15 μJ and 250 μm for the pump beam and 8 μJ and 150 μm for the probe beam. A backscattering geometry was employed to excite the sample and to acquire the Raman scattered light that was imaged through the entrance slit of a 0.5-m spectrograph whose grating dispersed the light onto a liquid nitrogen-cooled CCD detector.

Spectra of the photoproducts were found by subtraction of scaled probe-before-pump and scaled net solvent measurements from a pump−probe spectrum so as to delete the ground-state dihalomethane Raman bands and residual solvent Raman bands, respectively. The spectra were calibrated with an estimated uncertainty of ±5 cm^{-1} in absolute frequency using the known Raman shifts of the solvent Raman bands. The samples of dihalomethanes were prepared in solvents with varying water/acetonitrile concentrations (0/100%, 25/75%, 50/50%, and 75/25% by volume). The samples exhibited less than a few percent decomposition during the experiments, as found from UV/vis spectra taken before and after the ps-TR^3 measurements.

Ab Initio Calculations. The MP2 method was used to investigate the CH_2X-I (X = Cl, Br, I) + nH_2O (where $n = 1$, 2, 3) and $CH_2X(OH)$ + nH_2O (where $n = 0$, 1, 2, 3) reactions. The 6-31+G** basis set for all C, H, O, Cl, and Br atoms and the 6-311G** basis set for the I atom were used for both the geometry optimization and frequency calculations (analytically). The frequency calculations for the $CH_2I-I + 2H_2O$, $CH_2I-I + 3H_2O$ and $CH_2IOH + 4H_2O$ systems were done numerically because of limited computational resources. All of the calculations utilized the Gaussian 98 program suite.[76] IRC calculations were done to confirm that the transition states connected the appropriate reactants and products.[77,78] The Cartesian coordinates, total energies, and vibrational zero-point energies for the computed structures are given in the Supporting Information.

Results and Discussion

Photochemistry Experiments. Figure 1 presents UV−vis spectra obtained following 266-nm laser photolysis for varying times of 1×10^{-4} M CH_2I_2, CH_2BrI, and CH_2ClI in water solvent. The parent dihalomethane absorption bands (280−320 nm region for CH_2I_2 and 250−300 nm region for CH_2BrI and CH_2ClI) decrease in intensity with increasing photolysis time while those due to the I^- ion in the 225-nm region increase in intensity as the photolysis time. In the case of CH_2BrI, the increase in the I^- absorption band is accompanied by an increase in an absorption band at about 195 nm assigned to the Br^- ion. Examination of Figure 1 shows that there is a clear isobestic point near 253 nm between the parent absorption band(s) and the I^- absorption band for all three dihalomethanes, indicating that the I^- is formed directly from the dihalomethane parent molecules. The pH values of the sample solutions were also

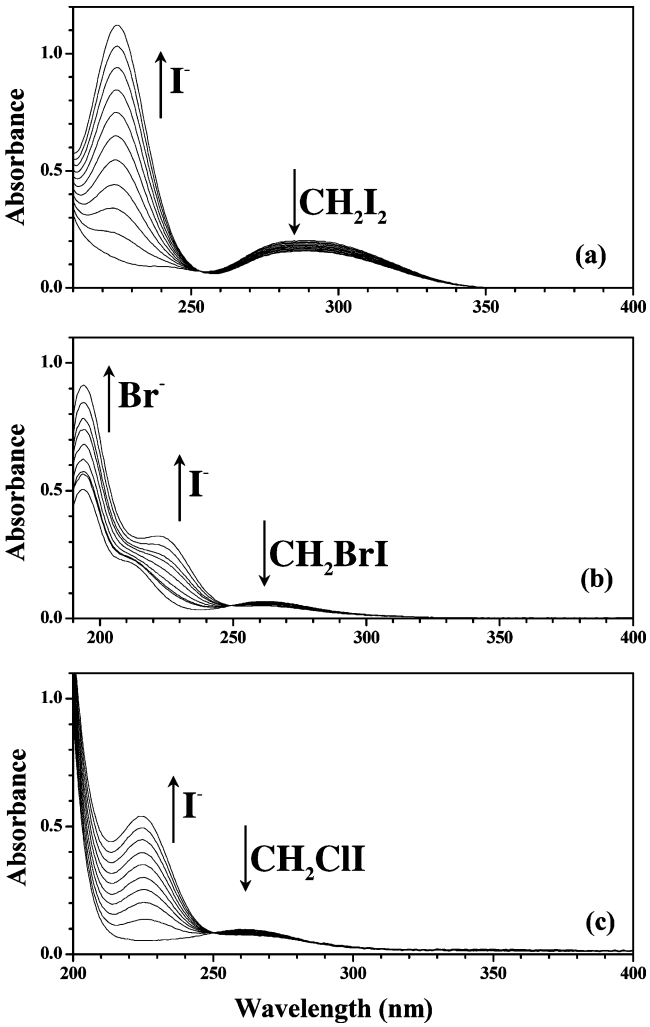

Figure 1. Absorption spectra obtained after different 266-nm photolysis times of about 1×10^{-4} M CH_2I_2 (a), CH_2BrI (b), and CH_2ClI (c) in pure water. The parent dihalomethane absorption bands decrease with increasing photolysis time and new absorption bands due to I^- appear at about 225 nm. In the case of CH_2BrI, a new absorption band due to Br^- appears at about 200 nm.

measured at the same time the absorption spectra were obtained and used to find $\Delta[H^+]$. The molar extinction coefficients of the dihalomethanes I^- and Br^- were used in conjunction with the absorption spectral changes to find $\Delta[CH_2XI]$ where X = I, Br, Cl, $\Delta[I^-]$, and $\Delta[Br^-]$ as the photolysis time varies. Plots of $\Delta[I^-]$ versus $-\Delta[CH_2XI]$ where X = I, Br, Cl as well as $\Delta[Br^-]$ versus $-\Delta[CH_2BrI]$ during the photochemistry experiments are depicted in the left column of Figure 2. Inspection of Figure 2 reveals that the increase in $[I^-]$ versus the decrease in $[CH_2XI]$ has a linear relationship, with slopes of about 2.0 $\pm$ 0.1 for CH_2I_2, 1.1 $\pm$ 0.1 for CH_2BrI, and 0.9 $\pm$ 0.1 for CH_2ClI. These results indicate that photolysis of CH_2XI at low concentrations in water releases two I^- for each CH_2I_2 and one I^- for CH_2BrI and CH_2ClI. The plots of $\Delta[H^+]$ versus $\Delta[I^-]$ shown in the right column of Figure 2 also display a linear relationship with slopes of about 1.1 $\pm$ 0.1 for CH_2I_2, 2.2 $\pm$ 0.2 for CH_2BrI, and 1.8 $\pm$ 0.2 for CH_2ClI. These results indicate that one H^+ is formed for each I^- following photolysis of low concentrations of CH_2I_2 in water. However, about two H^+ are produced for each I^- after photolysis of low concentrations of CH_2BrI and CH_2ClI in water. Why are the mixed dihalomethanes different from those of CH_2I_2? It is instructive to examine the change in the Br^- concentration versus the changes in the parent compound and H^+ concentrations for the CH_2BrI system shown at the bottom of Figure 2. The plots of $\Delta[Br^-]$ versus $-\Delta[CH_2BrI]$ and $\Delta[H^+]$ versus $\Delta[Br^-]$ have linear relationships with slopes of about 0.9 $\pm$ 0.1 and 2.2 $\pm$ 0.2, respectively. These results indicate that one Br^- ion is released following photolysis of low concentrations of CH_2BrI in water. This, combined with the changes of the pH and I^- and parent CH_2BrI concentrations, indicates that photolysis of low concentrations of CH_2BrI in water produces $2H^+$, Br^-, and I^- products. These final products are likely formed from HI and HBr leaving groups that dissociate into H^+ and I^- and H^+ and Br^-, respectively, in water.

To probe the fate of the carbon atom from the photolysis of the dihalomethanes at low concentrations in water, we performed the same ultraviolet photolysis experiments and used ^1H NMR to examine the products produced. Figure 3 displays ^1H NMR spectra obtained before, during, and after almost complete photolysis of low concentrations of CH_2XI (where X = I, Br, Cl) in D_2O solvent. In all three cases, photolysis of the dihalomethane produces a methandiol product ($CH_2(OD)_2$). These results are in agreement with previous ^1H and ^{13}C NMR experiments for the photolysis of low concentrations of diiodomethane (CH_2I_2 and $^{13}CH_2I_2$) in water solutions.[75]

The preceding photochemistry results suggest that the major reaction taking place after ultraviolet photolysis of low concentrations of CH_2XI where X = Cl, Br, I in water is the following overall reaction:

$$CH_2XI + h\nu n H_2O \rightarrow CH_2(OH)_2 + HI + HX + (n-2)H_2O \quad (1)$$

We note that previous experiments for CH_2I_2 using a Hg lamp source of light gave essentially the same results as for the unfocused nanosecond laser excitation (the reader is referred to ref 75 for details). This suggests that the photoproducts observed in Figures 1−3 are produced mostly from one photoexcitation of the dihalomethanes. To better understand the intermediates involved in the chemistry leading to the final products observed in the photochemistry experiments, ps-TR^3 spectroscopy experiments were done, and this is presented in the next section.

Picosecond Time-Resolved Resonance Raman Spectroscopy. Figure 4 presents selected ps-TR^3 spectra acquired using a 400-nm probe wavelength after 267-nm photolysis of CH_2I_2, CH_2BrI, and CH_2ClI in 100% CH_3CN, 50% H_2O/50% CH_3CN, and 75% H_2O/25% CH_3CN by volume solutions. The full range of ps-TR^3 spectra obtained at many more time delays used for following the kinetics of the intermediates species is given in the Supporting Information. The ps-TR^3 spectra are similar to those previously obtained in various solvents for isopolyhalomethane intermediates after 267-nm photolysis of the dihalomethanes in the condensed phase.[46,47,49,52,53,55,58,75] The vibrational assignments for the intermediate formed within several picoseconds and decaying on the hundreds of picoseconds time scale are readily assigned to isodihalomethanes that have been previously studied using time-resolved resonance Raman spectroscopy. For vibrational assignments of the isodiiodomethane (CH_2I-I) species formed after photolysis of CH_2I_2 in liquid solutions, the reader is referred to refs 47, 55, and 58 for details of the assignments. For the isobromoiodomethane (CH_2Br-I) species, the reader is referred to refs 46, 49, and 53 for details of the vibrational assignments. For the vibrational assignments of the isochloroiodomethane (CH_2Cl-I) species, the reader is referred to ref 52.

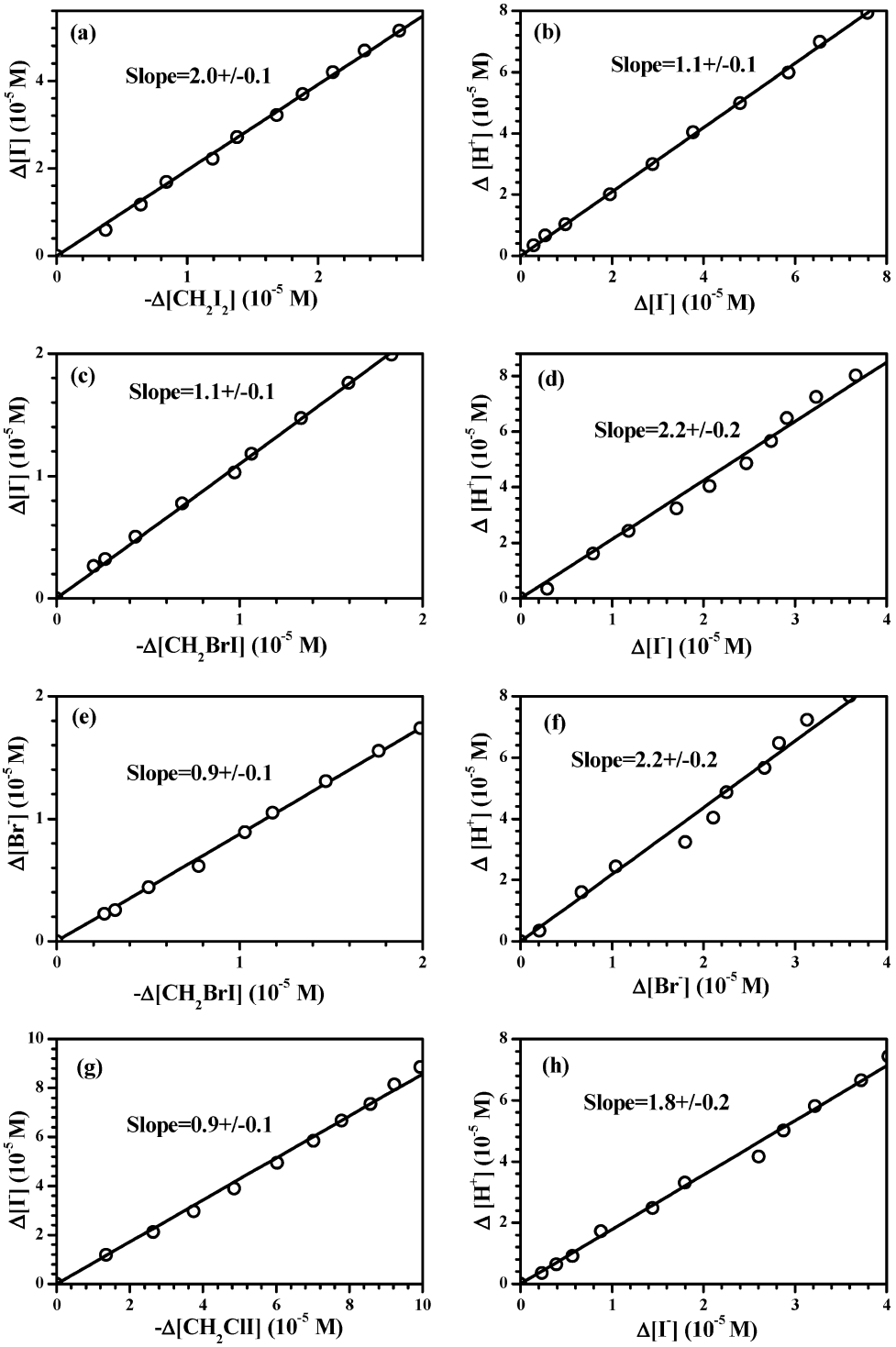

Figure 2. (Left) Plots of $\Delta[I^-]$ versus $-\Delta[CH_2I_2]$, $-\Delta[CH_2BrI]$, and $-\Delta[CH_2ClI]$, and a plot of $\Delta[Br^-]$ versus $-\Delta[CH_2BrI]$ derived from the absorption spectra shown in Figure 1. (Right) Plots of $\Delta[H^+]$ obtained from the pH measurements versus $\Delta[I^-]$ or $\Delta[Br^-]$ from the absorption spectra of Figure 1. Best fits of the data to a linear regression are displayed as lines with the slopes of the lines indicated next to the lines. See text for more details.

The CH_2I-I Raman band near 715 cm^{-1} assigned to the fundamental of the nominal C−I stretch mode (ν_3), the CH_2Br-I Raman bands in the 600−800 cm^{-1} region assigned to the fundamentals of the nominal C−Br stretch (ν_3), and CH_2 wag (ν_4) modes and the CH_2Cl-I Raman band near 725 cm^{-1} assigned to the fundamental of the nominal C−Cl stretch mode were integrated at different times to determine the kinetics of the growth and decay of the isodihalomethane species (CH_2X-I). Figure 5 presents plots of the relative integrated area of the ν_3 Raman band of the CH_2I-I species from 0 to 6000 ps, the ν_3 and ν_4 Raman bands of CH_2Br-I from 0 to 3000 ps, and the ν_4 Raman band of the CH_2Cl-I species from 0 to 1500 ps. In Figure 5, the open circles, solid triangles, and open squares represent data obtained in 100% CH_3CN, 50% H_2O/50% CH_3CN, and 75% H_2O/25% CH_3CN by volume solutions, respectively. These relative integrated areas of the relevant Raman bands were fit to a simple function (solid, dashed, and dotted lines in Figure 5):

$$I(t) = A\exp(-t/t_1) - B\exp(-t/t_2) \qquad (2)$$

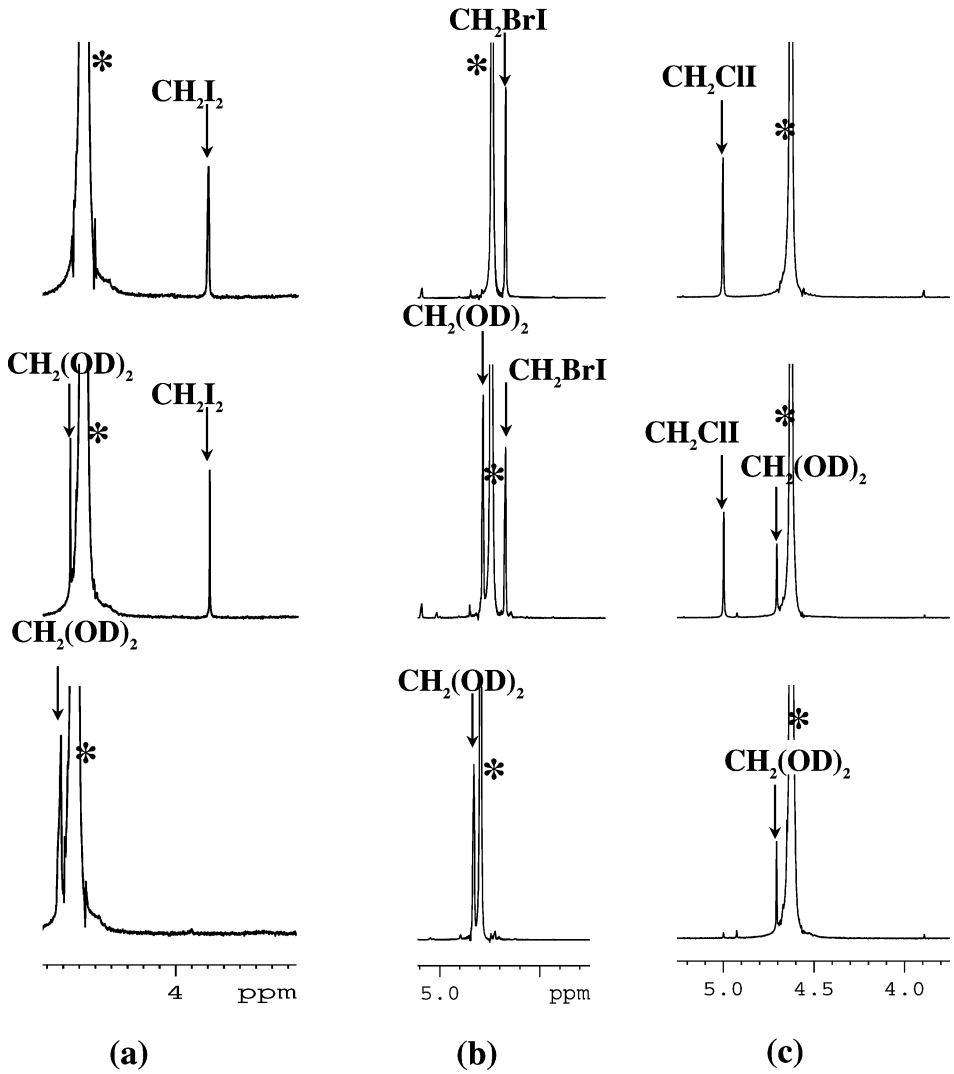

Figure 3. ^{1}H NMR spectra obtained before (top), during (middle), and after complete (bottom) 266-nm photolysis of CH_2I_2 (a), CH_2BrI (b), and CH_2ClI (c) in D_2O solution. In all three cases, photolysis converts the dihalomethane into a methanediol product ($CH_2(OD_2)$). See text for more details.

where $I(t)$ is the relative integrated area of the relevant isodihalomethane Raman band, t is the time, t_1 is the decay time constant of the relevant isodihalomethane Raman band, t_2 is the growth time constant of the relevant isodihalomethane Raman band, and A and B are constants. The fits to the data in Figure 5 found that the CH_2I-I species had decay time constants (t_1) of about 4640, 1860, and 680 ps in the 100% CH_3CN, 50% H_2O/50% CH_3CN, and 75% H_2O/25% CH_3CN by volume solutions, respectively. Similarly, the CH_2Br-I species had decay time constants (t_1) of about 2260, 296, and 130 ps and the CH_2Cl-I species had decay time constants (t_1) of about 120, 32, and 20 ps in the 100% CH_3CN, 50% H_2O/50% CH_3CN, and 75% H_2O/25% CH_3CN by volume solutions, respectively. In the pure acetonitrile solvent, the lifetime of the CH_2X-I species decreases noticeably as X changes from I to Br and then to Cl. This indicates that the CH_2X-I becomes less stable as X becomes more electronegative and is in agreement with the relative stability of these species in low-temperature matrixes where CH_2I-I started to disappear at temperatures above 100 K while CH_2Cl-I started to disappear at only 26−30 K.[39,40] As the percentage of water increases in the solvent system, the isopolyhalomethane intermediate observed in the ps-TR^3 spectra of Figure 4 decays substantially faster. This significantly faster decay for the CH_2I-I species as the water concentration increases was attributed to an O−H insertion reaction of CH_2I-I with water.[75] Our present results suggest this is also likely the case for the CH_2Br-I and CH_2Cl-I species. As the water concentration goes from 0 to 75%, the decay of the CH_2Br-I species changes noticeably more (from 2260 to 130 ps) than that of the CH_2I-I species (from 4640 to 680 ps). This suggests that the CH_2Br-I species may be more reactive toward water than the CH_2I-I species. To explore the relative chemical reactivity of these CH_2X-I (X = Cl, Br, I) species, we have done a systematic ab initio study of their reactions with water, and this is presented in the next section.

Ab Initio Study of the $CH_2X-I + nH_2O$ with $n = 1, 2, 3$ and $CH_2X(OH) + nH_2O$ with $n = 0, 1, 2, 3$ Reactions Where X = Cl, Br, I. Figures 6−11 present the optimized geometry with selected bond length and bond angle parameters, and Figure 12 shows schematic diagrams of the relative energy profiles (in kilocalories per mole) obtained from MP2 calculations (using the 6-31+G** basis set for all the C, H, O, Cl, and Br atoms and the 6-311G** basis set for the I atom) for the reactants, reactant complexes, transition states, and product complexes for the reactions of CH_2X-I (X = Cl, Br, I) + nH_2O where n = 1, 2, 3 and $CH_2X(OH)$ (X = Cl, Br, I) + nH_2O where n = 0, 1, 2, 3, 4.

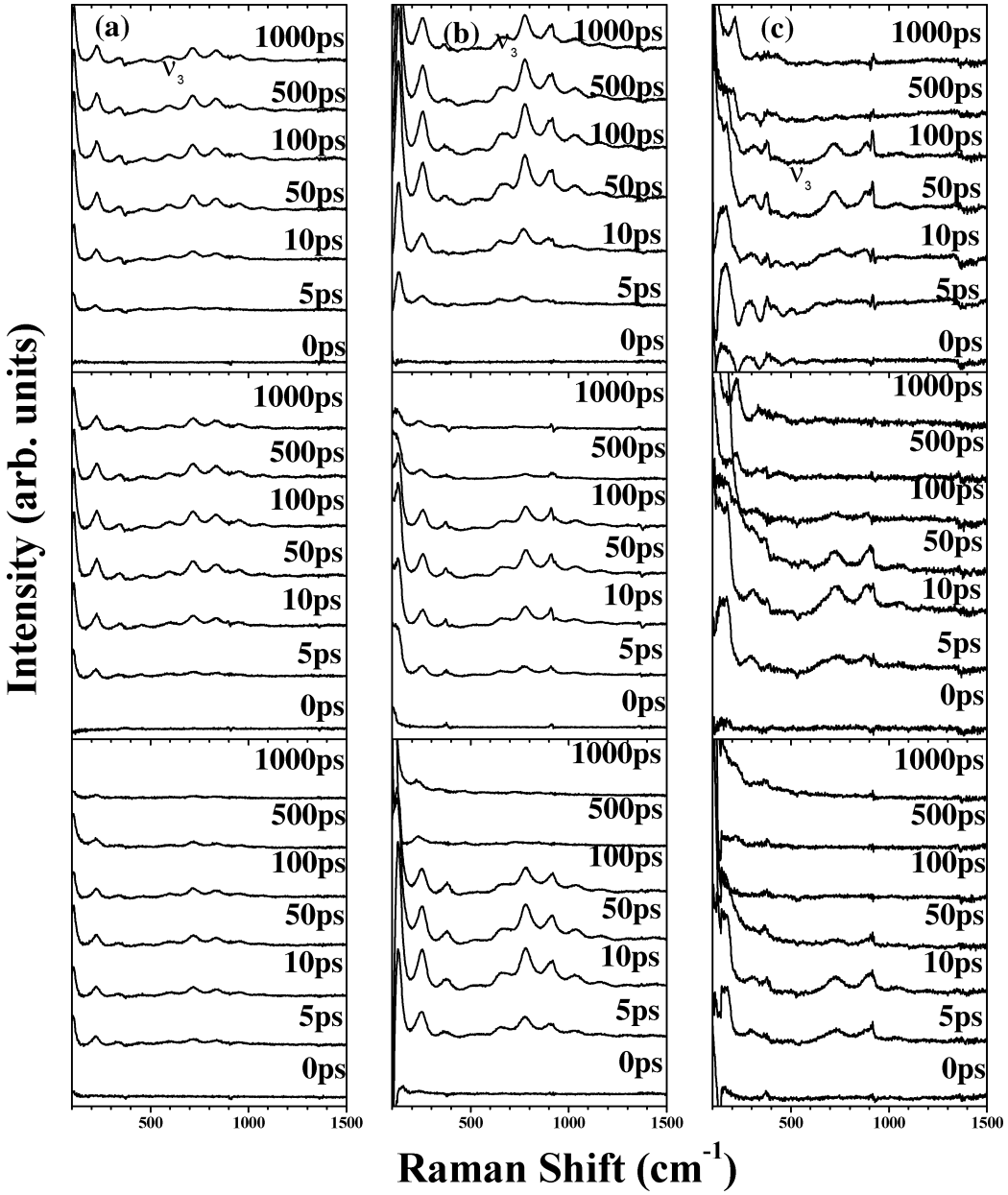

Figure 4. Stokes ps-TR^3 spectra (using a 400-nm probe wavelength) acquired after 267-nm photolysis of CH_2I_2 (a), CH_2BrI (b), and CH_2ClI (c) in 100% CH_3CN (top), 50% H_2O/50% CH_3CN (middle), and 75% H_2O/ 25%CH_3CN (bottom) solvents. Spectra were obtained at varying pump and probe time delays as indicated to the right of each spectrum (0, 5, 10, 50, 100, 500, and 1000 ps). Assignments are indicated for some of the larger isodihalomethane Raman bands. See text and refs 46, 47, 49, 52, 53, 55, and 58 for details of the assignments to the isodihalomethane species.

Inspection of Figures 6−8 shows there are some common systematic trends in the CH_2X-I (X = Cl, Br, I) + nH_2O reactions as the number of H_2O molecules increases. For the reactant complexes, the C−X bond length decreases (for example, the C−Br bond goes from 1.800 Å in RC1 to 1.789 Å in RC3 in the CH_2Br-I reaction system), the X−I bond length increases (for example, the Br−I bond goes from 2.883 Å in RC1 to 2.898 Å in RC3 in the CH_2Br-I reaction system), and the O···H−C distance decreases (for example, the O···H−C distance goes from 2.398 Å in RC1 to 2.122 Å in RC2 in the CH_2Br-I reaction system). Similarly, for the transition states, the C−X bond length decreases (for example, the C−Br bond goes from 1.768 Å in TS1 to 1.762 Å in TS3 in the CH_2Br-I reaction system) and the X−I bond length decreases (for example, the Br−I bond goes from 3.218 Å in TS1 to 3.074 Å in TS3 in the CH_2Br-I reaction system) in the transition states. In addition, the I−X−C angle increases (for example, the I−Br−C angle goes from 102.4° in TS1 to 121.2° in TS3 in the CH_2Br-I reaction system), and the C−O bond length increases (for example, the C−O bond goes from 2.131 Å in TS1 to 2.397 Å in TS3 in the CH_2Br-I reaction system) in the transition states. These changes in the RC and TS structures as the number of H_2O molecules increases can be mainly attributed to solvation of the terminal I atom with more hydrogen-bonding-like interactions while also interacting with the CH_2 group of the CH_2X-I species via the O···H−C interactions as has been seen previously in the CH_2I-I + nH_2O reactions.[75]

The changes in the structures taking place for the CH_2X-I + nH_2O reactions as they proceed from the RCs to the TSs (shown in Figures 6−8) indicate that the C−X bond becomes modestly stronger, the X−I bond noticeably weakens, and the C−O bond becomes partially formed. These changes are accompanied by the I···H interactions becoming moderately stronger that is consistent with some H−I bond formation. The changes observed as the RCs go to the TSs are consistent with an O−H insertion/HI elimination reaction occurring to form a

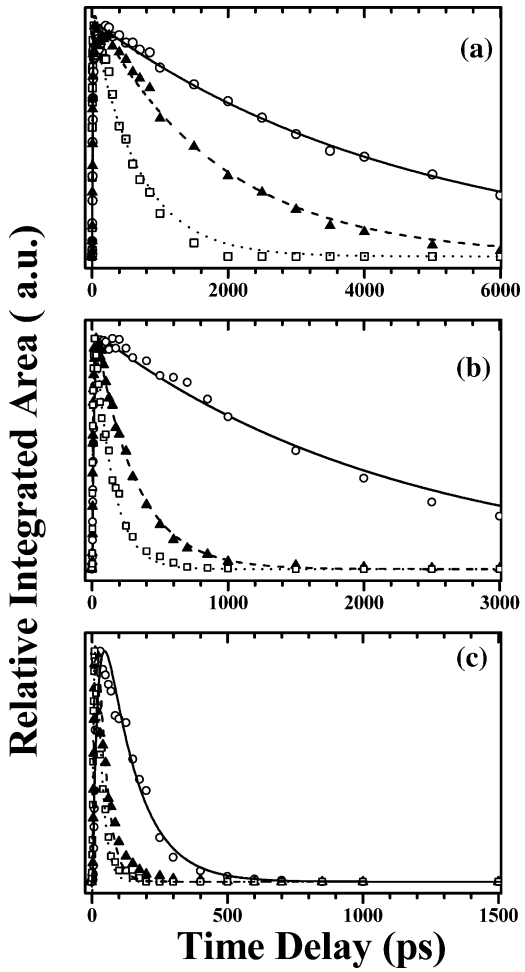

Figure 5. Plots of the relative integrated areas of the major isodihalomethane Raman bands (ν_3 Raman band for CH_2I-I (a), ν_n Raman band for CH_2Br-I (b), and ν_n Raman band for CH_2Cl-I (c)) at different delay times (from 0 to 6000 ps) obtained in 100% CH_3CN (○), 50% H_2O/50% CH_3CN (▲), and 75% H_2O/ 25%CH_3CN (□) solvents. The solid lines (100% CH_3CN), dashed lines (50% H_2O/50% CH_3CN), and dotted lines (75% H_2O/25% CH_3CN) represent least-squares fits to the data (see text for more details).

$CH_2X(OH)$ product and a HI leaving group. This was confirmed for selected reactions by IRC calculations, and the vibrational frequencies for the reaction coordinate were found to be 386i, 292i, and 133i cm^{-1}, respectively, for TS1, TS2, and TS3 of the $CH_2Br-I + nH_2O$ reaction system as an example. Inspection of Figure 12 shows that, as the number of H_2O molecules increases, the degree of stabilization is noticeably greater for the corresponding transition states, and this leads to systematically lower barriers for reaction from the reactant complexes to their transition states: 13.7 kcal/mol from RC1 to TS1, 8.7 kcal/mol from RC2 to TS2, and 2.6 kcal/mol from RC3 to TS3 for the $CH_2BrI + nH_2O$ reactions, for example. These results indicate that additional H_2O molecules significantly catalyze the $CH_2X-I + nH_2O \rightarrow CH_2X(OH) + HI + (n-1)H_2O$ reactions. As the RCs go toward the TSs, the I−X−C angle, the X−I bond length, and the C−O bond formation experience smaller changes as the number of H_2O molecules increases. For example, the I−Br−C angle undergoes a change of 15.3° from RC1 to TS1, 11.9° from RC2 to TS2, and 2.8° from RC3 to TS3 in the $CH_2Br-I + nH_2O$ reactions. Similarly, the Br−I bond length shows a change of 0.335 Å from RC1 to TS1, 0.280 Å from RC2 to TS2, and 0.176 Å from RC3 to TS3 in the $CH_2Br-I + nH_2O$ reactions. The C−O bond formation is weaker with C−O bond lengths of 2.131 Å for TS1, 2.228 Å for TS2, and 2.397 Å for TS3 in the $CH_2Br-I + nH_2O$ reactions. These changes in the I−X−C bond angle, X−I bond length, and the C−O bond formation all suggest that less energy is required to proceed from the RCs to their TSs as more H_2O molecules are added to the reaction system. This is consistent with the lower barriers to reaction observed as more H_2O molecules are involved in the $CH_2X-I + nH_2O$ reactions.

The changes in the structures of Figures 9−11 as the RCs go to their TSs indicate that the C−X bond becomes weaker, the O···H bond becomes partially formed in the O···H−O−C moiety of the $CH_2X(OH)$ molecule, and the X···H interactions usually become somewhat stronger. These changes are consistent with some H−X bond formation accompanied by a HX elimination reaction to produce a CH_2O product and an HX leaving group. This was confirmed by IRC calculations for selected reactions, and the vibrational frequencies for the reaction coordinate were found to be 498i, 408i, and 407i cm^{-1}, respectively, for TS1, TS2, and TS3 of the $CH_2Br(OH) + nH_2O$ reaction system as an example. Inspection of Figure 12 reveals that the degree of stabilization appears greater for the TSs, and this leads to systematically lower barriers to reaction from the RCs to the TSs as the number of H_2O molecules increases: 17.6 kcal/mol from RC1 to TS1, 13.5 kcal/mol from RC2 to TS2, and 5.6 kcal/mol from RC4 to TS4 for the $CH_2Br(OH) + nH_2O$ reactions, for example. This suggests that additional H_2O molecules significantly catalyze these reactions. As the RCs go to the TSs, the O−C−X angle, the C−O bond length, and the C−X bond length tend to show smaller changes as the number H_2O molecules increases. For example, the C−O bond length displays a change of −0.112 Å from RC1 to TS1, −0.114 Å from RC2 to TS2, −0.098 Å from RC3 to TS3, and −0.088 Å from RC4 to TS4, and the C−Br bond length changes by +0.691 Å from RC1 to TS1, +0.609 Å from RC2 to TS2, and +0.433 Å from RC4 to TS4 for the $CH_2Br(OH) + nH_2O$ reactions. These changes suggest that less energy is needed to proceed from the RCs to their corresponding TSs as more H_2O molecules are added and that this is consistent with the lower barriers to reaction as more H_2O molecules are involved in the $CH_2X(OH) + nH_2O \rightarrow CH_2O + HX + nH_2O$ reactions.

Water Catalysis, Solvation of the HI Leaving Group, and Variations as X Changes from Cl to Br to I in the $CH_2X-I + nH_2O$ ($n = 1, 2, 3$) and $CH_2X(OH) + nH_2O$ ($n = 0, 1, 2, 3, 4$) Reactions. It is illuminating to compare our present results to those previously obtained for neutral $I(H_2O)_n$ and $I^-(H_2O)_n$ complexes[79−81] as well as for the dissolution of HX strong acids by H_2O molecules.[82−87] The stabilization energies of the I atom were calculated to be about 0.5 kcal/mol for I···HOH and 1.65 kcal/mol for $I\cdots OH_2$, and these values are much smaller than the values for the I^- anion with H_2O that were calculated to be about −10.38 kcal/mol[81] or −9.43 kcal/mol.[80] The stabilization energies of the $(CH_2X-I)[H_2O]$ complexes were found to be in the 5.1−5.4 kcal/mol range and those of the $(CH_2X(OH))[H_2O]$ were found to be in the 7.3−7.7 kcal/mol range. These values are between those found for the neutral $I(H_2O)_n$ and $I^-(H_2O)_n$ complexes[80,81] and suggest that solvation of an I^--like moiety takes place in the $(CH_2X-I)[H_2O]$ and $(CH_2X(OH))[H_2O]$ RCs.

It is also instructive to compare our present results to those recently reported for the dissociation of HI in H_2O complexes.[85] This investigation found that the stabilization of the $HI(H_2O)_n$ clusters ranged from 4.02 kcal/mol for $n = 1$ to 56.97 kcal/mol for $n = 5$, similar to the trend observed for the $I^-(H_2O)_n$ clusters[80,81] and our results for the $(CH_2X-I)(H_2O)_n$ and $[CH_2X(OH)](H_2O)_n$ RCs and TSs shown in Figures 6−11. The average

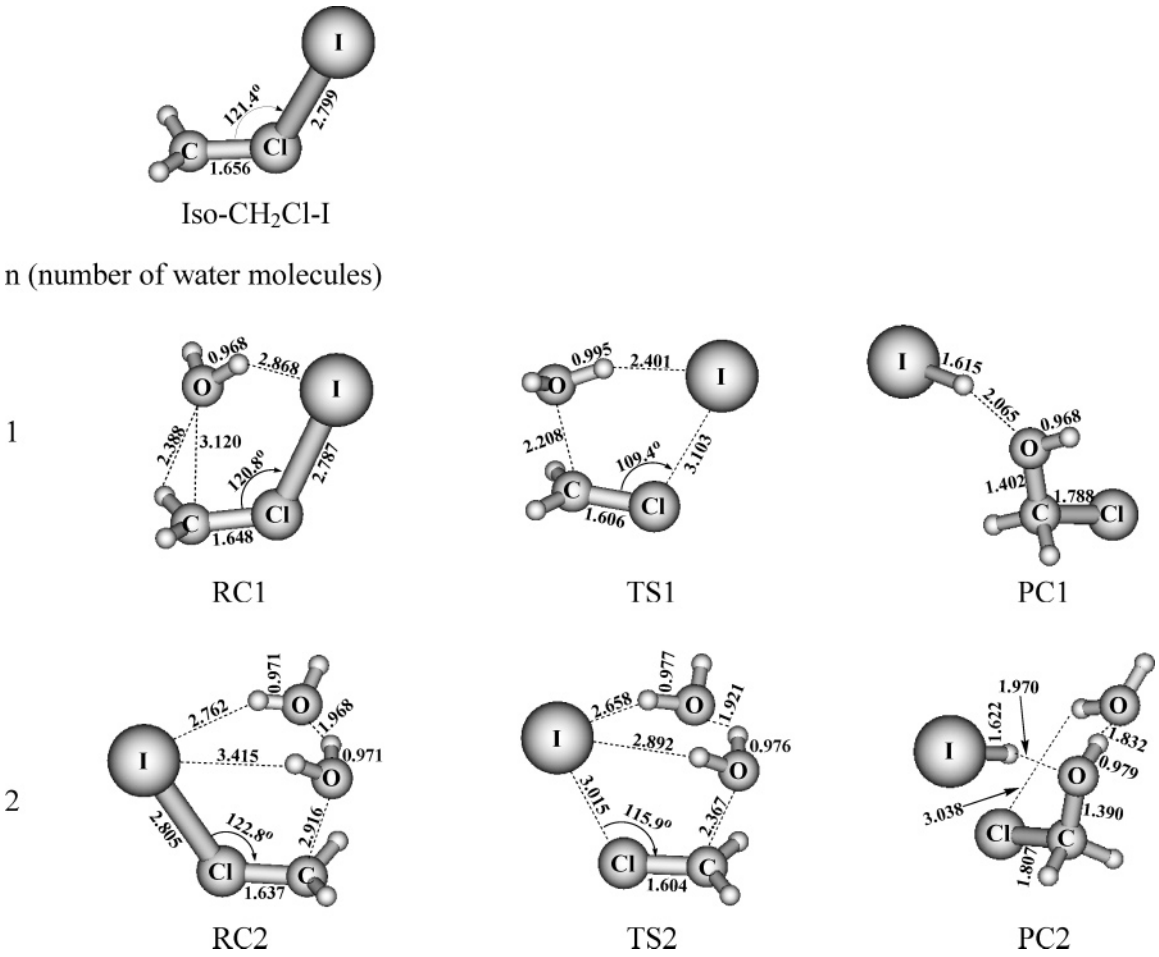

Figure 6. Schematic diagrams are shown for the reactants, reactant complexes, transition states (TS), product complexes (PC), and products for the reactions of $CH_2Cl-I + nH_2O$ where $n = 1, 2$. The optimized geometries for these species were obtained from MP2 calculations (employing the 6-31+G** basis set for all C, H, O, and Cl atoms and the 6-311G** basis set for the I atom). Selected bond length (in Å) and bond angle (in degrees) parameters are shown.

H···I distances were computed to be ~1.6 Å for $HI(H_2O)_n$, where $n = 0, 1, 2$, ~2.1 Å for $HI(H_2O)_3$ and ~2.5 Å for $HI(H_2O)_n$, where $n = 4, 5$, and suggest that HI remains nondissociated with addition of one or two H_2O molecules but becomes partially dissociated into a H_3O^+, I^- "ion-pair"-like species for the $HI(H_2O)_3$ complex and then is mostly dissociated in the $n = 4, 5$ $HI(H_2O)_n$ complexes.[85] The HX elimination reactions of the $[CH_2X(OH)](H_2O)_n$ species are similar to the dissociation of HI in the $HI(H_2O)_n$ complexes. For example, examination of the structures for the $(CH_2O)(HX)(H_2O)_n$ product complexes in Figures 9−11 shows that PC0 with no H_2O molecule and PC1 with one H_2O molecule have H−I bond distances of 1.614 and 1.619 Å, respectively, that are close to the ~1.6 Å value for a nondissociated HI molecule and H−Br distances of 1.428 and 1.441 Å, respectively, that are close to the ~1.4 Å value for a nondissociated HBr molecule. For the $(CH_2O)(HX)(H_2O)_n$ PCs with $n = 2$, the H···I distance becomes intermediate in range with a value of 2.239 Å for PC2 with X = I, consistent with partial dissociation into a H_3O^+, I^- "ion-pair"-like species similar to that found for the $HI(H_2O)_3$ complex,[85] and the H···Br distance becomes intermediate in range with a value of 1.893 Å for PC2 with X = Br, consistent with partial dissociation into a H_3O^+, Br^- "ion-pair"-like species similar to that found for the $HBr(H_2O)_3$ complex.[85] For the $(CH_2O)(HX)(H_2O)_4$ product complexes, the H···X distances become longer with values in the 2.4−2.7 Å range for PC4 with X = I, in the 2.1−2.4 Å range for PC4 with X = Br, and in the 1.97−2.1 Å range for PC4 with X = Cl, consistent with complete dissociation into $H_3O^+$and X^- species similar to that found for the $HX(H_2O)_n$ complexes where $n = 4$ and 5.

An NBO analysis was done for the RCs, TSs, and PCs in Figures 6−11. The terminal (or leaving) X atom has NBO charges of −0.537 and −0.620 for RC1 and RC2 of the $CH_2Cl-I + nH_2O$ reactions and −0.513, −0.548, and −0.610 for RC1−RC3, respectively, for the $CH_2Br-I + nH_2O$ reactions, and −0.546, −0.574, and −0.628 for RC1−RC3, respectively, for the $CH_2I-I + nH_2O$ reactions. The charges on the terminal I atom increase in the RCs as the number of water molecules increases, consistent with solvation of an I^--like moiety of the CH_2X-I species. The charge on the leaving group X atom of the $(CH_2O)(HX)(H_2O)_n$ product complexes in Figures 9−11 shows a good correlation with the nondissociated or dissociated character of the HX leaving group. For example, PC0 with no H_2O molecule and PC1 with one H_2O molecule have H−I bond distances and I atom charges of 1.614 Å and −0.128 and 1.619 Å and −0.161, respectively, that are consistent with a nondissociated HI molecule. Similarly, PC0 and PC1 have H−Br bond distances and Br atom charges of 1.428 Å and −0.271 and 1.441 Å and −0.305, respectively, that are consistent with a nondissociated HBr molecule. The $(CH_2O)(HX)(H_2O)_n$ PC with $n = 2$ and X = I has a longer H···I distance of 2.239 Å for PC2 and an I atom charge of −0.793, consistent with dissociation into a H_3O^+, I^- "ion-pair"-like species similar to that found for the $HI(H_2O)_3$ complex.[85] Similarly, the H···Br distance becomes 1.893 Å for PC2 and a Br atom charge of −0.749, consistent with dissociation into a H_3O^+, Br^- "ion-pair"-like species similar

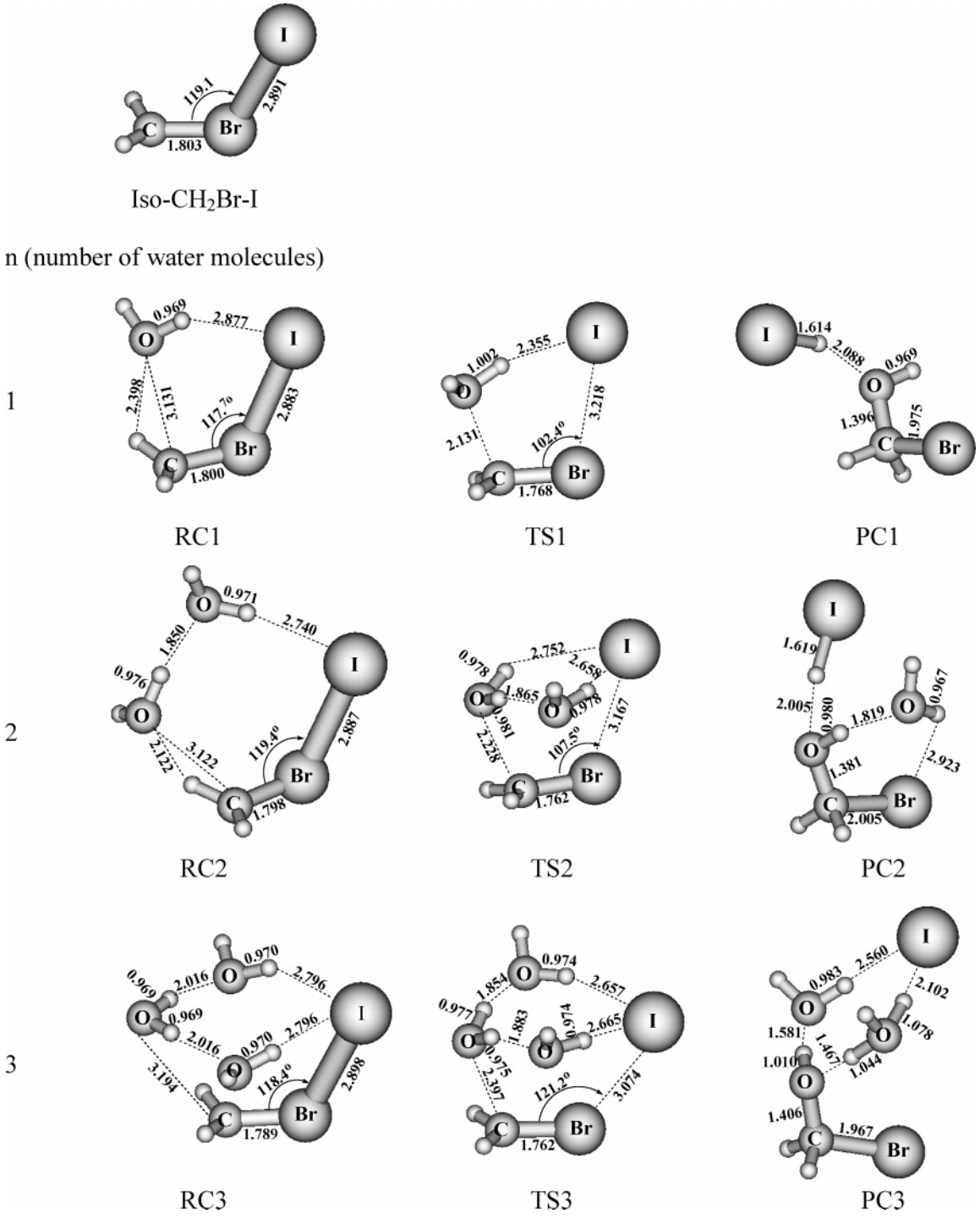

Figure 7. Schematic diagrams are shown for the reactants, reactant complexes, transition states, product complexes, and products for the reactions of $CH_2Br-I + nH_2O$ where $n = 1, 2, 3$. The optimized geometries for these species were obtained from MP2 calculations (employing the 6-31+G** basis set for all C, H, O, and Br atoms and the 6-311G** basis set for the I atom). Selected bond length (in Å) and bond angle (in degrees) parameters are shown.

to that found for the $HBr(H_2O)_3$ complex.[85] For the $(CH_2O)(HX)(H_2O)_4$ product complexes, the H···X distances become moderately longer with values in the 2.4−2.7 Å range for PC4 with X = I, 2.1−2.4 Å for PC4 with X = Br, and 1.97−2.1 Å for PC4 with X = Cl, and the charges on the X atoms are in the −0.817 to −0.832 range, consistent with complete dissociation into $H_3O^+$and X^- species similar to that found for the $HX(H_2O)_n$ complexes where $n = 4$ and 5.[85] It is interesting to note that the transition from a nondissociated HX molecule to a dissociated H_3O^+ X^- ion pair does not occur until four H_2O molecules in the $(CH_2O)(HX)(H_2O)_4$ product complexes compared to about two or so H_2O molecules for the X = Br and I complexes.

It is worth noting some interesting differences between the dissociation of HX in the $HX(H_2O)_n$ complexes and the water-catalyzed HX elimination reactions investigated in this report. For instance, the proton is transferred from the HX molecule to the O atom of a water molecule in the dissociation of HX in the $HX(H_2O)_n$ complexes while the proton is transferred from the OH group of the $CH_2X(OH)$ molecule in the $[CH_2X(OH)](H_2O)_n$ water-catalyzed HX elimination reactions, and this results in the proton on the O−H group being shared with a

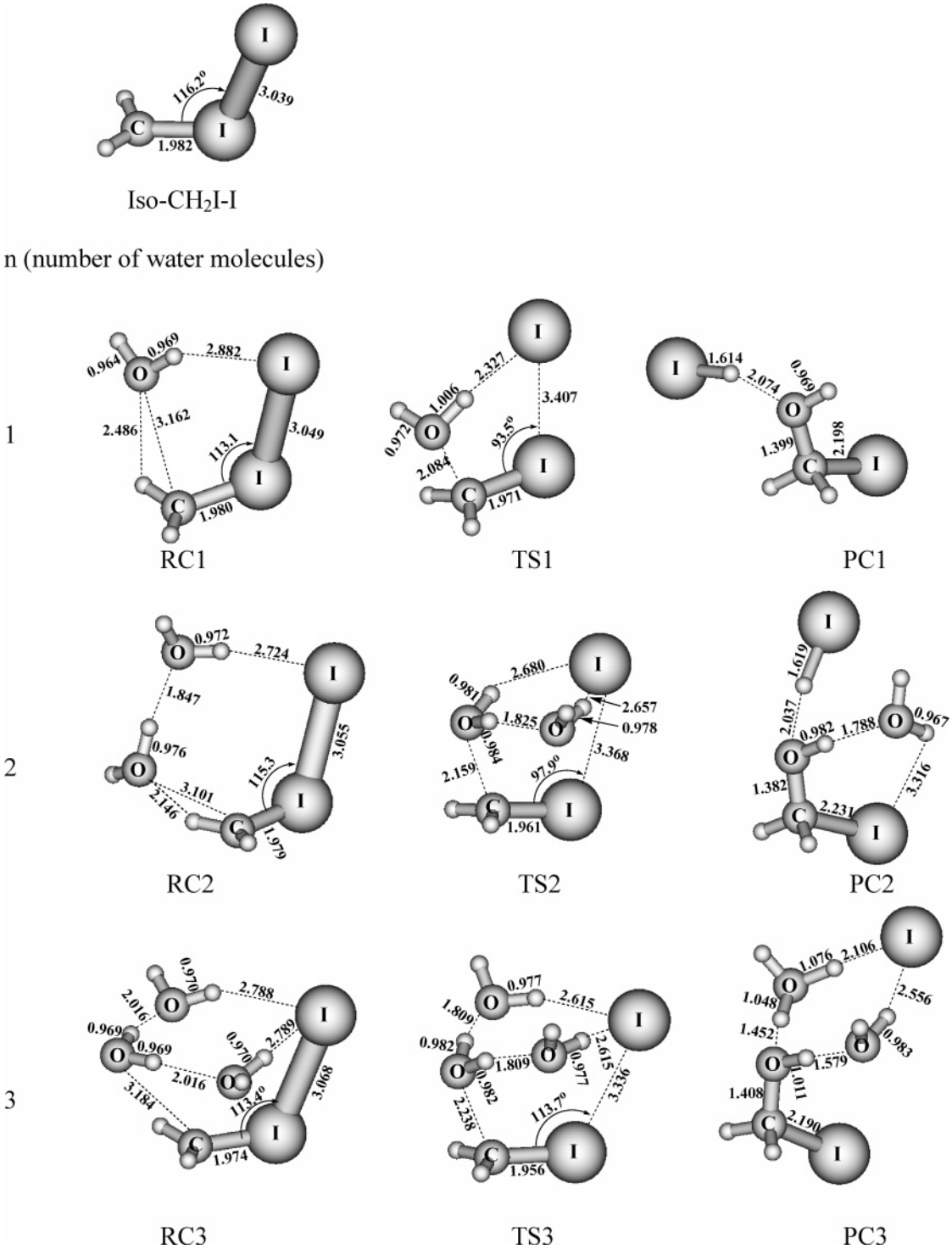

Figure 8. Schematic diagrams are shown for the reactants, reactant complexes, transition states, product complexes, and products for the reactions of $CH_2I-I + nH_2O$ where $n = 1, 2, 3$. The optimized geometries for these species were obtained from MP2 calculations (employing the 6-31+G** basis set for all C, H, and O atoms and the 6-311G** basis set for the I atoms). Selected bond length (in Å) and bond angle (in degrees) parameters are shown.

H_2O molecule in the transition states (TS1−TS4) of the $[CH_2X(OH)](H_2O)_n$ water-catalyzed HX elimination reactions. The HI elimination and dissociation processes in the $CH_2X-I(H_2O)_n$ reactions are coupled to the O−H insertion reaction with H_2O. This leads to the C−O bond formation of the H_2O molecule being coupled to a proton transfer to another H_2O molecule and the solvation of the terminal I atom (and cleavage of the X−I bond) of the CH_2X-I species. This suggests that the water-catalyzed solvation and dissociation of a HX or a similar leaving group may be coupled to help drive other reactions. The ability of employing water to catalyze other reactions by utilizing an appropriate leaving group(s) would probably be useful for a range of potential applications and of general interest for synthetic chemists.

There are several interesting trends in the $CH_2X-I + nH_2O$ ($n = 1, 2, 3$) and $CH_2X(OH) + nH_2O$ ($n = 1, 2, 3, 4$) reactions as the identity of X changes from Cl to Br to I. The barriers to reaction from the RCs to their respective TSs become larger as X goes from Cl to Br to I in the $CH_2X-I + nH_2O$ ($n = 1, 2, 3$) reactions. For example, the barriers to reaction for the

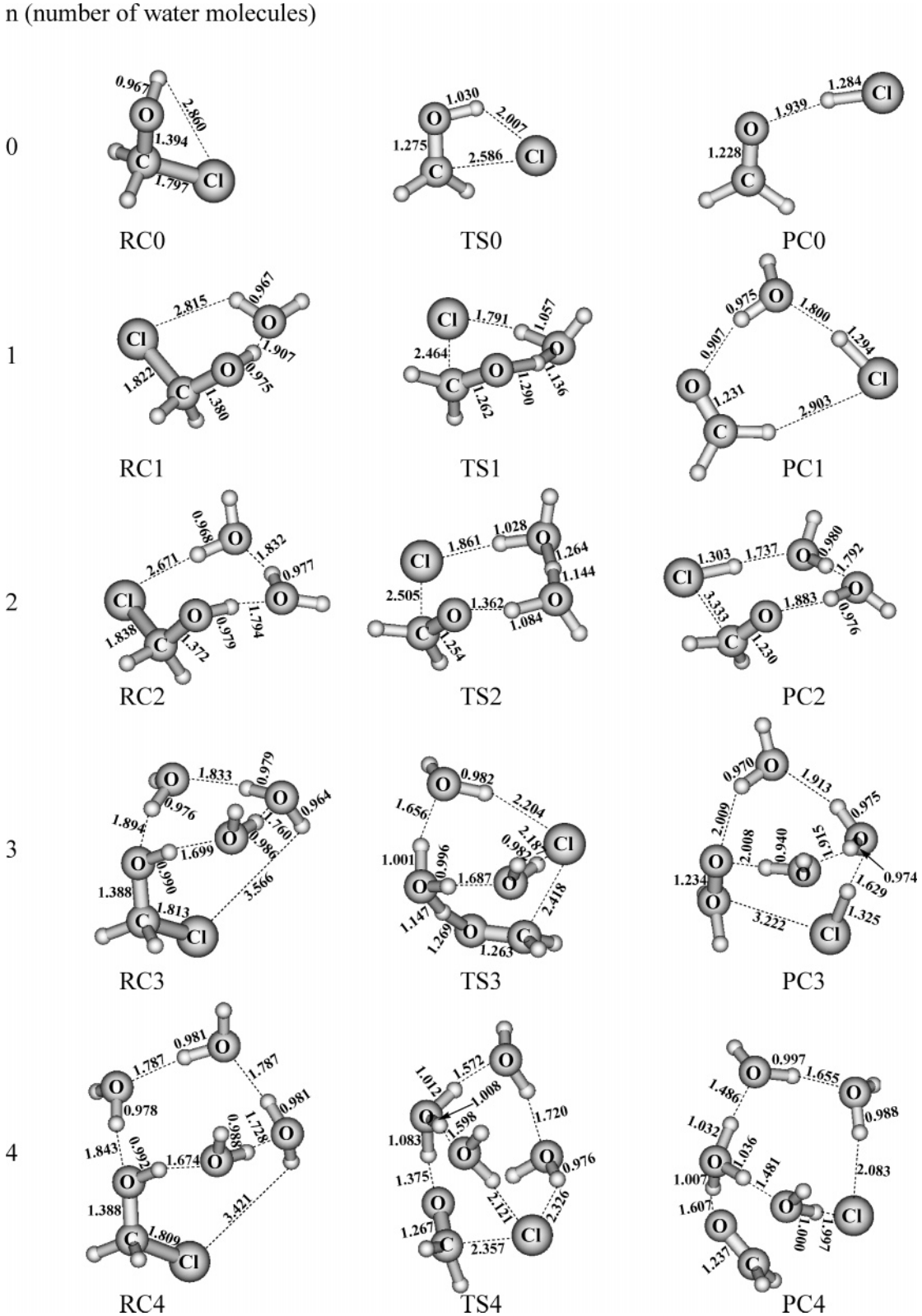

Figure 9. Schematic diagrams are shown for the reactants, reactant complexes, transition states, product complexes, and products for the reactions of $CH_2Cl(OH) + nH_2O$ where $n = 0, 1, 2, 3, 4$. The optimized geometries for these species were obtained from MP2 calculations (employing the 6-31+G** basis set for all C, H, O, and Cl atoms). Selected bond length (in Å) and bond angle (in degrees) parameters are shown.

$CH_2X-I + nH_2O$ ($n = 1$) are 8.7 kcal/mol for X = Cl, 13.7 kcal/mol for X = Br, and 17.2 kcal/mol for X = I. This trend is the same as the number of water molecules involved in the reaction increases. For example, the barriers to reaction for the $CH_2X-I + nH_2O$ ($n = 2$) are 2.7 kcal/mol for X = Cl, 8.7 kcal/mol for X = Br, and 12.9 kcal/mol for X = I. For the $CH_2X-I + nH_2O$ ($n = 3$) reactions, they are 2.6 kcal/mol for X = Br and 5.9 kcal/mol for X = I. These calculated trends for the $CH_2X-I + nH_2O$ ($n = 1, 2, 3$) reactions are consistent with the apparent reactivity of the CH_2X-I species with water in the ps-TR[3] experiments where the reactivity follows the order of $CH_2Cl-I > CH_2Br-I > CH_2I-I$. As the water concentration

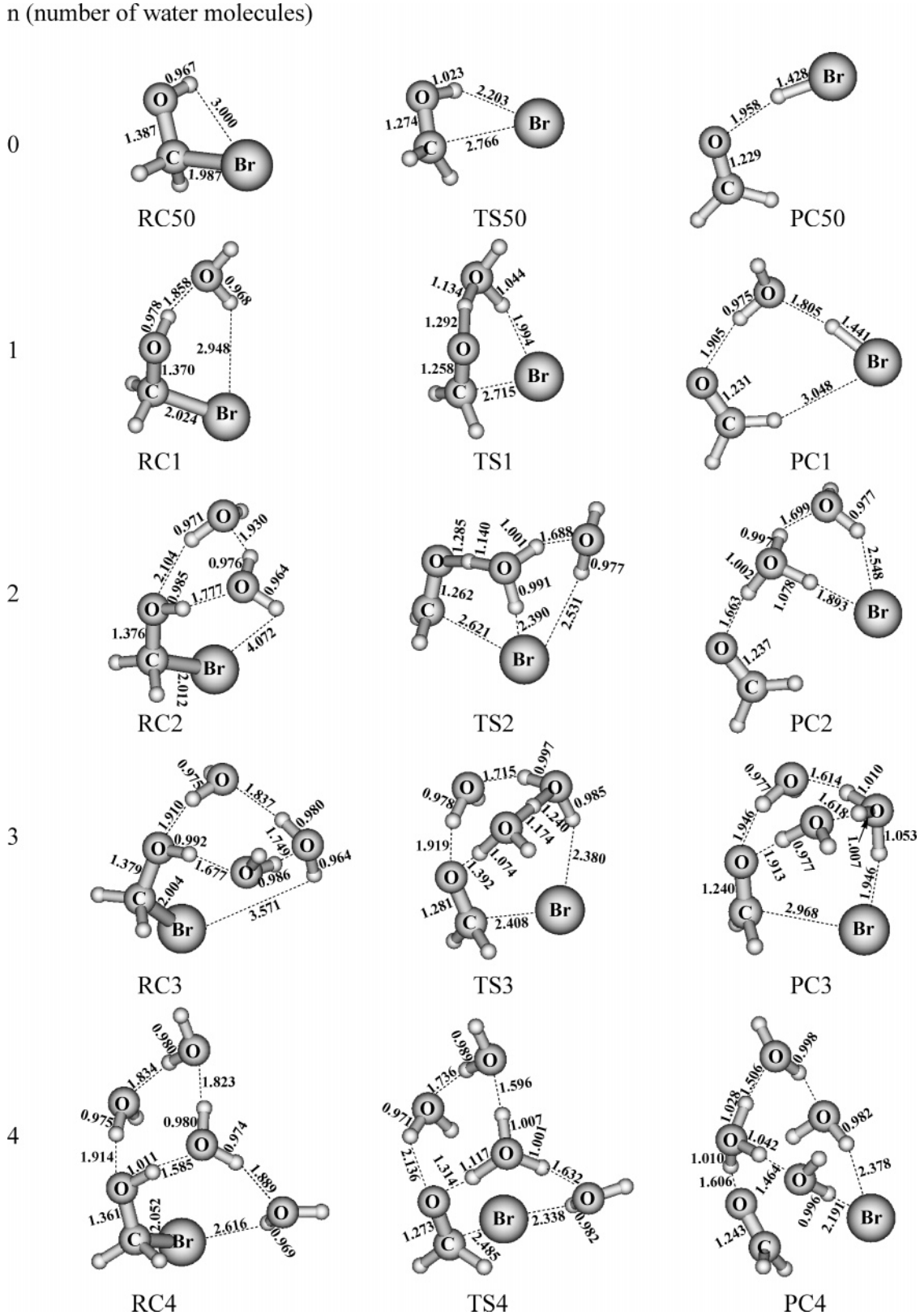

Figure 10. Schematic diagrams are shown for the reactants, reactant complexes, transition states, product complexes, and products for the reactions of $CH_2Br(OH) + nH_2O$ where $n = 0, 1, 2, 3, 4$. The optimized geometries for these species were obtained from MP2 calculations (employing the 6-31+G** basis set for all C, H, O, and Br atoms). Selected bond length (in Å) and bond angle (in degrees) parameters are shown.

goes from 0 to 75%, the decay of the CH_2Cl-I changes from 120 to 20 ps, the CH_2Br-I species changes from from 2260 to 130 ps, and the CH_2I-I species from 4640 to 680 ps. In pure acetonitrile solvent, the lifetime of the CH_2X-I species decreases noticeably and X changes from I (4640 ps) to Br (2260 ps) and then Cl (120 ps), indicating that the CH_2X-I becomes less stable as X becomes more electronegative in agreement with the relative stability of these species in low-temperature matrixes where CH_2I-I started to disappear at temperatures above 100 K while CH_2Cl-I started to disappear at only 26−

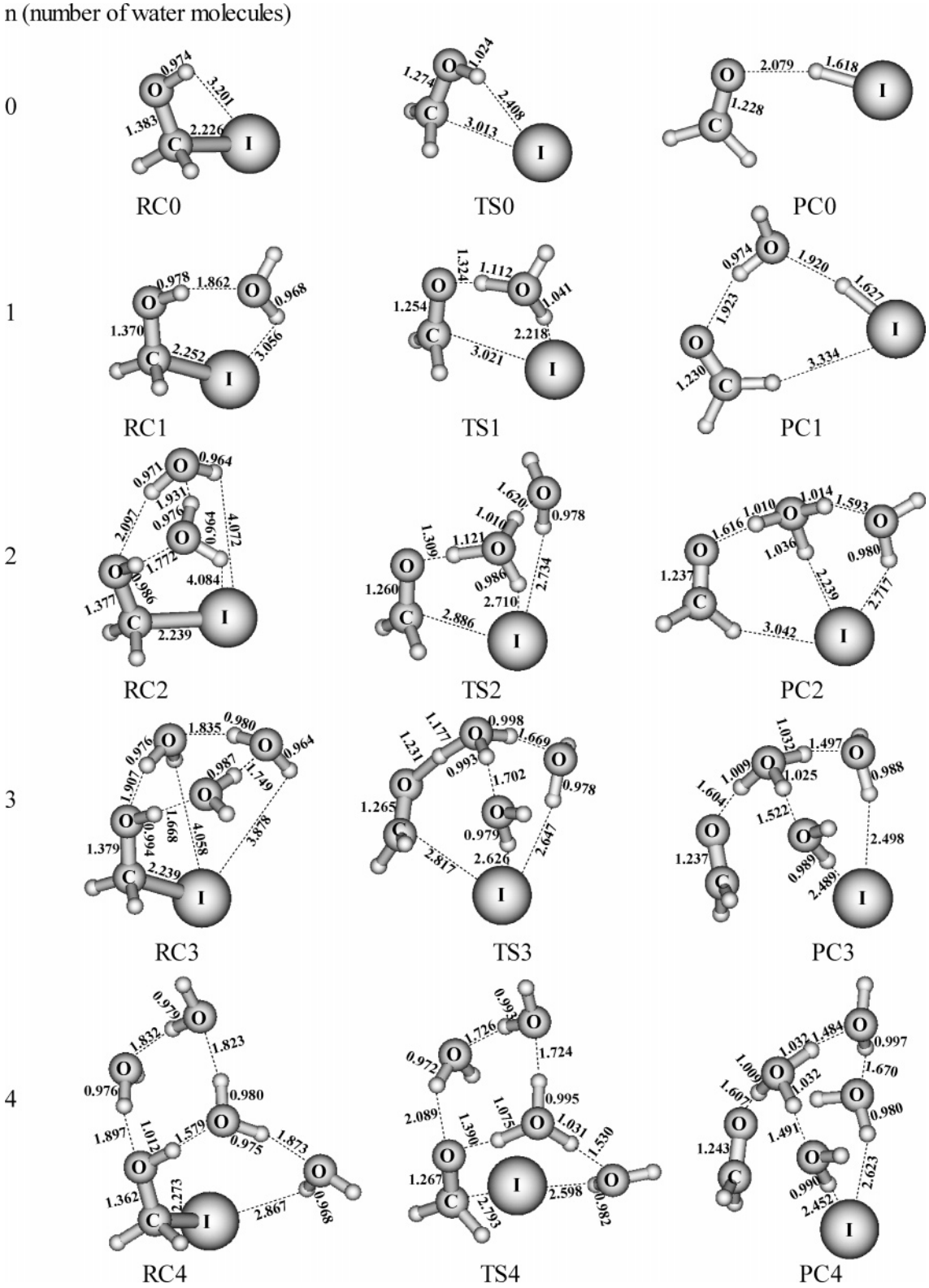

Figure 11. Schematic diagrams are shown for the reactants, reactant complexes, transition states, product complexes, and products for the reactions of $CH_2I(OH) + nH_2O$ where $n = 0$, 1, 2, 3, 4. The optimized geometries for these species were obtained from MP2 calculations (employing the 6-31+G** basis set for all C, H, and O atoms and the 6-311G** basis set for the I atom). Selected bond length (in Å) and bond angle (in degrees) parameters are shown.

30 K.[39,40] If the CH_2Cl-I species had a chemical reactivity similar to that for CH_2Br-I and CH_2I-I, then one could expect that its short 120-ps lifetime in pure acetonitrile would not change much as the concentration of water goes from 0 to 75%. If the chemical reactivity of CH_2Cl-I toward water was significantly greater than that of CH_2Br-I and CH_2I-I, then its short lifetime could change significantly as the water concentration increases from 0 to 75%; this is the behavior that is experimentally observed in the ps-TR[3] experiments. Similarly, the chemical reactivity of CH_2Br-I appears greater than that of CH_2I-I where the CH_2Br-I species lifetime (from 2260 to 130 ps) becomes substantially shorter than that of CH_2I-I

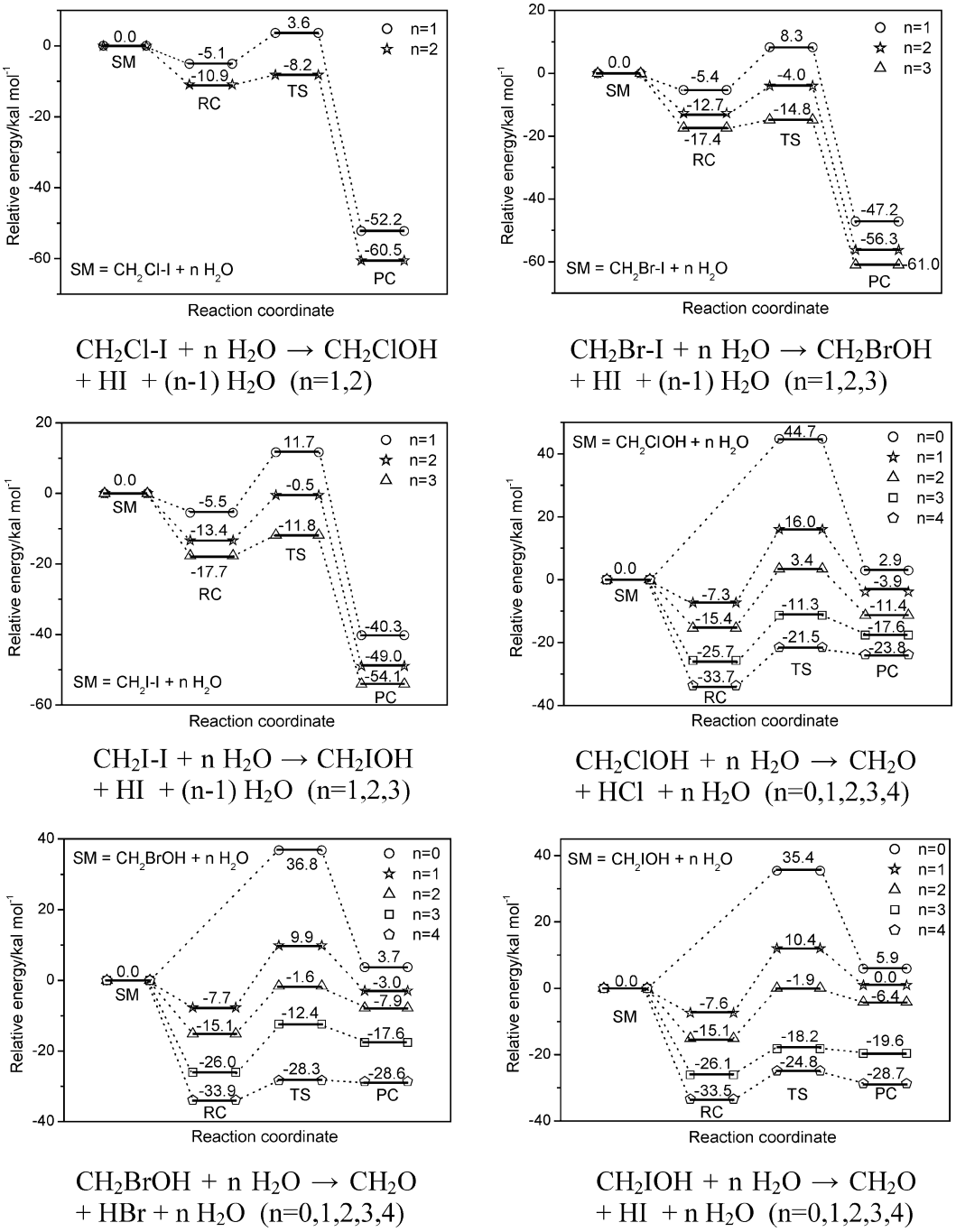

Figure 12. (a) Schematic diagrams of the relative energy profiles (in kilocalories per mole) obtained from the MP2 calculations (employing the 6-31+G** basis set for all C, H, O, Cl, and Br atoms and the 6-311G** basis set for the I atoms) for the reactions of CH_2X-I (X = I, Br, Cl) + nH_2O where n = 1, 2, (3). (b) Schematic diagrams of the relative energy profiles (in kilocalories per mole) obtained from the analogous MP2 calculations for the reactions of $CH_2X(OH)$ (X = I, Br, Cl) + nH_2O where n = 0, 1, 2, 3, 4.

lifetime (from 4640 to 680 ps) as the water concentration increases from 0 to 75% water.

The trends in the barriers to reaction for $CH_2X-I + nH_2O$ (n = 1, 2, 3) as X changes from Cl to Br to I correlate in general to structural changes in the RCs and TSs in the ab initio computational results. For example, as the RCs go toward the TSs, the I−X−C angle and the X−I bond length experience greater changes and the C−O bond formation becomes greater as X goes from Cl to Br to I. For example, the I−X−C angle undergoes changes of 11.4° for X = Cl, 15.3° for X = Br, and 19.6° for X = I, and the X−I bond length changes 0.316 Å for X = Cl, 0.335 Å for X = Br, and 0.358 Å from RC1 to TS1. The C−O bond formation is greater as X goes from Cl to Br to I with C−O bond lengths of 2.208 Å for X = Cl, 2.131 Å for X = Br, and 2.084 Å for X = I in TS1 in the $CH_2X-I + H_2O$ reactions. Similar trends for the changes in the I−X−C angles, the X−I bond lengths, and C−O bond formation also occur for X = Cl to Br to I as the number of H_2O molecules increases. For example, the $CH_2X-I + 2H_2O$ reactions have I−X−C angle changes of 6.9° for X = Cl, 11.9° for X = Br, and 17.4° for X = I and X−I bond length changes of 0.099 Å for X = Cl, 0.280 Å for X = Br, and 0.313 Å from RC2 to TS2 with C−O bond lengths of 2.367 Å for X = Cl, 2.228 Å for X = Br, and 2.159 Å for X = I in TS2. These changes in the I−X−C bond angle, X−I bond length, and the C−O bond formation all suggest that more energy is required to proceed from the

RCs to their TSs as X changes from Cl to Br to I in the reaction system. This is consistent with the higher barriers to reaction observed as X changes from Cl to Br to I in the $CH_2X-I + nH_2O$ reactions.

The trends in the $CH_2X(OH) + nH_2O$ ($n = 1, 2, 3, 4$) reactions are significantly different from those of the $CH_2X-I + nH_2O$ ($n = 1, 2, 3$) reactions as the identity of X changes from Cl to Br to I. While the barrier height goes up for the $CH_2X-I + nH_2O$ ($n = 1, 2, 3$) reactions as the identity of X changes from Cl to Br to I, the barrier height for the $CH_2X(OH) + nH_2O$ ($n = 1, 2, 3, 4$) reactions goes down as X changes from Cl to Br to I. For example, the barrier to reaction decreases from about 23 kcal/mol for X = Cl to about 18 kcal/mol for X = Br and I for the $CH_2X(OH) + H_2O$ reactions. The same trend is observed as the number of water molecules involved in the reaction increases. For example, the barrier to reaction decreases from 14.4 kcal/mol for X = Cl to 13.6 kcal/mol for X = Br to 7.9 kcal/mol for X = I for the $CH_2X-I + 3H_2O$ reactions. This trend is probably mostly due to the differing strengths of the carbon−halogen (C−X) bonds that need to be broken in the HX elimination reactions. This could also account for an interesting trend in the structural properties of the product complexes produced from the $CH_2X(OH) + nH_2O$ ($n = 1, 2, 3, 4$ and X = Cl, Br, I) reactions. Inspection of the structures of the product complexes (PC1−PC4) in Figures 9−11 for the $CH_2X(OH) + nH_2O$ ($n = 1, 2, 3, 4$ and X = Cl, Br, I) reactions reveals the $H_3O^+ X^-$ ion-pair-like formation in the PCs does not occur until four H_2O molecules are involved in the reaction for X = Cl in contrast to two H_2O molecules for the PCs of X = Br and X = I. The C−Cl bond is much stronger than the C−Br and C−I bonds, and thus one would expect that much more of the solvation energy of the coupled HX dissolution reaction would be needed to drive the overall $CH_2X(OH)$ HX elimination reaction. In this case, the corresponding formation of the $H_3O^+ Cl^-$ ion pair would be expected to occur after more water molecules are involved in the reaction, compared to the reactions where the weaker C−Br and C−I bonds are broken. Both the trends in the barrier heights to the $CH_2X(OH) + nH_2O$ ($n = 1, 2, 3, 4$) reactions and the structural parameters of the PCs formed from these reactions as X changes from Cl to Br to I are consistent with the water catalysis of the HX elimination reactions and the coupled HX dissolution in water driving the $CH_2X(OH)$ HX elimination reactions.

Proposed Reaction Mechanism for the $CH_2XI + h\nu + nH_2O \rightarrow CH_2(OH)_2 + HI + HX + (n - 2)H_2O$ Overall Reaction. We propose the following reaction mechanism for the $CH_2XI + h\nu + n(H_2O) \rightarrow CH_2(OH)_2 + HI + HX + (n - 2)H_2O$ overall reaction (where X = Cl, Br, I) that we observe for 266-nm photolysis of low concentrations of CH_2XI in aqueous solutions: Photolysis of CH_2XI To Form CH_2X and I Fragments

$$\text{Step 1} \qquad CH_2XI + h\nu \rightarrow CH_2I + I$$

Solvent-Induced Geminate Recombination of the CH_2X and I Fragments To Form the CH_2X-I Isomer

$$\text{Step 2} \qquad CH_2X + I \rightarrow CH_2X-I$$

Water-Catalyzed O−H Insertion/HI Elimination Reaction of CH_2X-I with H_2O Solvent

Step 3

$$CH_2X-I + n(H_2O) \rightarrow CH_2X(OH) + HI + (n - 1)H_2O$$

Water-Catalyzed HX Elimination Reaction of $CH_2X(OH)$ with H_2O Solvent

$$\text{Step 4} \qquad CH_2X(OH) + n(H_2O) \rightarrow H_2CO + HX + n(H_2O)$$

Water (and/or Acid)-Catalyzed Addition of H_2O to H_2CO in H_2O Solvent

$$\text{Step 5} \qquad H_2CO + n(H_2O) \rightarrow CH_2(OH)_2 + (n - 1)H_2O$$

Add Steps 1−5 To Obtain This Overall Reaction

$$\mathbf{CH_2XI + h\nu + n(H_2O) \rightarrow CH_2(OH)_2 + HI + HX + (n - 2)H_2O}$$

Ultraviolet excitation of CH_2XI (where X = Cl, Br, I) in both gas and solution phases typically results in direct cleavage of the C−I bond to produce CH_2X radical and I atom fragments.[22−38,41−43] This provides some evidence that step 1 in the above reaction mechanism is the primary photochemical start of the reaction. The initially produced CH_2X radical and I atom fragments can undergo solvent-induced geminate recombination to form a CH_2X-I isomer species within a few picoseconds.[41−43,47,50,52,53] This indicates that step 2 of the proposed reaction mechanism happens to an appreciable extent in room-temperature solutions. Our ps-TR^3 experiments show that CH_2X-I is produced to an appreciable extent in largely aqueous solutions and has a substantially shorter lifetime with increasing water concentrations (this work and also refs 55 and 75), and this suggests that CH_2X-I is reacting with H_2O molecules. This behavior is consistent with the proposed step 3 of the reaction mechanism. Our present ab initio calculations indicate that CH_2X-I reacts with H_2O via a water-catalyzed O−H insertion/HI elimination reaction to produce $CH_2X(OH)$ and HI products consistent with the proposed step 3 of the reaction mechanism. The $CH_2X(OH)$ and HI products do not absorb substantially at the 400-nm probe wavelength used in the ps-TR^3 experiments done in largely aqueous solutions (this work and refs 55 and 75). Thus, these species would not likely be observed under these conditions consistent with the ps-TR^3 results.[55,75] Recent ps-TR^3 experiments showed that the isobromoform species reacts with water to directly produce a $CHBr_2(OH)$ product species,[73,74] and this provides direct vibrational spectroscopic evidence that isopolyhalomethanes can undergo O−H insertion reactions with H_2O molecules. In so far as the CH_2X-I species have similar chemical reactivity, these results for the isobromoform species provide additional experimental support for step 3 in our proposed reaction mechanism.

Our current ab initio computations indicate that $CH_2X(OH)$ undergoes water-catalyzed HX elimination to produce H_2CO and HX products consistent with step 4 in the proposed reaction mechanism. We note that the chloromethanol [$CH_2Cl(OH)$] species has been observed in low-temperature matrix isolation experiments[88] and in gas-phase experiments[89,90] and in all cases was found to decompose in the dark to H_2CO and HCl products, with the decomposition of chloromethanol [$CH_2Cl(OH)$] being accelerated by heterogeneous processes in the gas-phase studies.[89,90] These experimental results are consistent with step 4 of the proposed reaction mechanism and our present ab initio calculations for the HX elimination reaction of $CH_2X(OH)$.

It is well-known that formaldehyde (H_2CO) in aqueous solution undergoes water addition to produce methanediol [$CH_2(OH)_2$],[91−93] and this strongly supports step 5 in the proposed reaction mechanism in that any H_2CO produced in an aqueous environment will almost certainly go on to produce

methanediol [$CH_2(OH)_2$]. It is intriguing that a theoretical study of this reaction indicates that it may proceed mostly through a cooperative mechanism with three H_2O molecules hydrating the carbonyl group.[94] This cooperative mechanism appears similar to the water-catalyzed CH_2X-I O−H insertion/HI elimination and $CH_2X(OH)$ HX elimination reactions of steps 3 and 4 examined here. Since the H_2CO product is formed with a nearby solvated HX leaving group in step 4, this could possibly acid-catalyze the water addition reaction of step 5. We expect that conversion of H_2CO to methanediol [$CH_2(OH)_2$] takes place quickly in aqueous solutions in the proposed reaction mechanism.

The proposed reaction mechanism presented here helps explain how photolysis of low concentrations of CH_2XI in aqueous solution leads to production of HI + HX leaving groups and a $CH_2(OH)_2$ molecule that are the main photolysis products observed by our ^{13}C NMR, ^1H NMR, IR, UV/vis, and pH photochemistry results. Our current ab initio results indicate that there are low barriers to reaction for the water-catalyzed CH_2X-I O−H insertion/HI elimination reactions and $CH_2X(OH)$ HX elimination reactions of steps 3 and 4. This and the known chemistry of H_2CO in aqueous solutions for step 5 indicate that the very reactive CH_2X-I species would probably be efficiently converted into the HI + HX and $CH_2(OH)_2$ final products.

Possible Implications for the Decomposition of Polyhalomethanes and Halomethanols in Water-Solvated Environments. Ultraviolet photolysis at wavelengths greater than 260 nm of CH_2XI (where X = Cl, Br, I) in the gas phase leads mostly to cleavage of the C−I bond to form CH_2X radical and I fragments with a near unity quantum yield.[22−38] In contrast, our present investigation found that 266-nm ultraviolet photolysis of low concentrations of CH_2XI in aqueous solution results in conversion of the parent molecule into HI + HX and $CH_2(OH)_2$ products. This indicates that the photochemistry of CH_2XI (X = Cl, Br, I) displays significant phase dependence with substantially different reactions occurring in aqueous solution compared to the gas phase. The reaction mechanism shown in the preceding section that includes the O−H insertion/HI elimination reactions of CH_2X-I with water and the subsequent HX elimination reactions of $CH_2X(OH)$ with water in conjunction with the known hydrolysis of formaldehyde can explain how the ultraviolet photolysis of CH_2XI in aqueous solution dehalogenates to produce the HI + HX and $CH_2(OH)_2$ products. The water-catalyzed reactions of CH_2X-I with water and the subsequent $CH_2X(OH)$ reaction of $CH_2X(OH)$ HX elimination reactions may be noticeable sources of halogens and/or aid formation in the natural environment. These types of water-catalyzed HX elimination reactions of isopolyhalomethanes and halomethanols have not been considered to our knowledge for the water-solvated photochemistry of polyhalomethanes (from natural and/or man-made sources) that have been observed in the natural environment.

A range of isopolyhalomethanes has been observed after ultraviolet photolysis of their respective polyhalomethane in largely aqueous solutions.[55,73−75] These isopolyhalomethanes may be able to react with water to release strong acids as was found here for the CH_2X-I reactions with water. This suggests that the pH in the solvated aqueous environment around the parent polyhalomethane becomes more acidic and may possibly influence reactions associated with the activation of halogens in aqueous sea-salt particles where several proposed reaction schemes depend on pH.[10−21] For halogen activation processes on aqueous sea-salt particles, it has been proposed that H^+ and X^- can help activate the halogen atom via reactions such as $HOX + H^+ + X^- \rightarrow X_2 + H_2O$ (where X = Cl and/or Br) and/or $HOX^- + H^+ \rightarrow X + H_2O$.[10−20]

Our present work indicates that photolysis of CH_2XI (where X = Cl, Br, I) in aqueous solution releases HI and HX groups. We speculate that if this happens in aqueous sea-salt particles the HI or HX released may cause analogous reactions to activate halogens such as by the $HOX + H^+ + I^- \rightarrow XI + H_2O$ reaction. Photolysis of CH_2BrI in aqueous solution produces both HBr and HI similar to producing 2HI groups from ultraviolet photolysis of CH_2I_2. In the case of CH_2BrI and likely CH_2ClI, the possible activation of I would be accompanied by Cl or Br and probably cause additional ozone destruction via their known synergistic pathways. Ultraviolet photolysis of CH_3I in aqueous solution does not appear to release noticeable acid groups, and this is likely due to its inability to make an isopolyhalomethane from its two initially produced photofragments in condensed-phase environments. We note that the photochemistry of CH_2I_2 and CH_2BrI was found to be responsible for most of the IO observed in the marine boundary layer of the troposphere, while CH_3I made very little contribution even though it is present in greater amounts (mean concentration of 0.43 pptv compared to 0.08 and 0.05 pptv for CH_2I_2 and CH_2BrI, respectively).[7,8] We speculate that the aqueous-phase photochemistry of CH_2I_2 and CH_2BrI that releases strong acids with the potential for halogen activation in sea-salt particles could possibly account for why the photochemistry of CH_2I_2 and CH_2BrI is mainly responsible for the formation of IO in the marine boundary layer, while the CH_3I molecule (which does not have the isopolyhalomethane chemistry and its strong acid release) does not have much contribution to the IO being formed from the photochemistry of these halogenated methanes. Ultraviolet photolysis of several polyhalomethanes in aqueous solutions has been observed to release strong acids with reasonable quantum yields[73−75,95] via their isopolyhalomethane chemistry. Therefore, we think it would be useful to undertake additional studies to better understand how this water-solvated chemistry may actually influence the chemistry of the natural environment (particularly for reactions that are acid-catalyzed or affected by pH such as halogen activation in heterogeneous environments).

Halomethanols such as bromomethanol and chloromethanol could possibly be formed in the atmosphere by reaction of hydroxymethyl radicals (CH_2OH) with atomic or molecular halogens in the gas phase.[9] Thus, halomethanols may possibly act as a halogen reservoir in the atmosphere.[9] Chloromethanol decays into HCl and H_2CO products and has a lifetime of at least a 100 s (and probably much longer) because of homogeneous decomposition in the gas phase and also to decay much faster on surfaces.[89,90] Our current ab initio calculations for the reaction of halomethanols ($CH_2X(OH)$) indicate that their decomposition can be greatly accelerated even by reaction with one water molecule and further accelerated by additional H_2O molecules, suggesting that decomposition of halomethanols will be sensitive to the humidity of the atmosphere and decompose very fast in solvated water environments (like the interfacial and/or bulk regions of water and ice particles). It may be worthwhile to study the reaction rates for halomethanols with H_2O in the gas phase, on surfaces, and in bulk aqueous solutions so as to better understand their decomposition in the natural environment. Our present and recent ab initio work for the CH_2I-I reactions with water[75] coupled with the direct observation of the O−H insertion reaction of isobromoform to produce the $CHBr_2OH$ molecule[73,74] indicate that halomethanols can be produced in noticeable amounts from the photochemistry of polyhalomethanes in solvated aqueous environments. This new

photochemical route to produce halomethanols can be used to examine the relatively unknown chemistry of halomethanols in condensed-phase environments.

Conclusions

A combined experimental and theoretical examination of the ultraviolet photolysis of CH_2XI (where X = Cl, Br, I) dihalomethanes in water was given. Ultraviolet photolysis of low concentrations of CH_2XI (where X = Cl, Br, I) in water was found to give almost complete conversion into $CH_2(OH)_2$ and HX and HI products. Picosecond time-resolved resonance Raman (ps-TR^3) spectroscopy experiments showed that CH_2X-I isodihalomethane intermediates were made within several picoseconds after photolysis of the CH_2XI parent compound in mixed aqueous solutions. The decay of the CH_2X-I intermediates became noticeably shorter as the water concentration increased, suggesting that they may be reacting with water. Ab initio calculations indicate that the CH_2X-I intermediates can react relatively easily with water via water-catalyzed O−H insertion/HI elimination reactions to form $CH_2X(OH)$ and HI products. The barrier for these reactions was found to increase as X changes from Cl to Br to I. The ab initio calculations also indicate that the $CH_2X(OH)$ product can undergo a water-catalyzed HX elimination reaction to produce $H_2C{=}O$ and HX products. The barrier for these reactions was found to decrease as X changes from Cl to Br to I. The preceding two water-catalyzed reactions can account for the HI and HX leaving groups observed experimentally. The $H_2C{=}O$ product reacts further with water to form the other $CH_2(OH)_2$ product observed in the photochemistry experiments. These results suggest that that the CH_2X-I intermediates react with water to form the $CH_2(OH)_2$ and HI and HX products measured in the photochemistry experiments. Ultraviolet photolysis of CH_2XI (where X = Cl, Br, I) at low concentrations in water results in efficient dehalogenation and release of two strong acid (HI and HX) leaving groups. The potential effect of this photochemistry of CH_2XI dihalomethanes in water on their decomposition in aqueous and possibly natural environments was very briefly discussed.

Acknowledgment. This work was supported by grants from the Research Grants Council (RGC) of Hong Kong (HKU 7036/04P) and (HKU 1/01C) to D.L.P. W.M.K. thanks the University of Hong Kong for the award of a postdoctoral fellowship.

Supporting Information Available: Figures S1−S9 showing the ps-TR^3 spectra obtained after 267-nm photolysis of CH_2X-I (X = Cl, Br, I) in 100% CH_3CN, 50% H_2O/50% CH_3CN, and 75% H_2O/25% CH_3CN by volume solutions. The Cartesian coordinates, total energies, and vibrational zero-point energies are presented for selected stationary structures shown in Figures 6−11. This material is available free of charge via the Internet at http://pubs.acs.org.

References and Notes

(1) Class, Th.; Ballschmiter, K. *J. Atmos. Chem.* **1988**, *6*, 35−46.
(2) Klick, S.; Abrahamsson, K. *J. Geophys. Res.* **1992**, *97*, 12683−12687.
(3) Heumann, K. G. *Anal. Chim. Acta* **1993**, *283*, 230−245.
(4) Moore, R. M.; Webb, M.; Tokarczyk, R.; Wever, R. *J. Geophys. Res., C: Oceans* **1996**, *101* (9), 20899−20908.
(5) McElroy, C. T.; McLinden, C. A.; McConnell, J. C. *Nature* **1997**, *397*, 338−341.
(6) Mössigner, J. C.; Shallcross, D. E.; Cox, R. A. *J. Chem. Soc., Faraday Trans.* **1998**, *94*, 1391−1396.
(7) Carpenter, L. J.; Sturges, W. T.; Penkett, S. A.; Liss, P. S. *J. Geophys. Res., D: Atmos.* **1999**, *104*, 1679−1689.
(8) Alicke, B.; Hebstreit, K.; Stutz, J.; Platt, U. *Nature* **1999**, *397*, 572−573.
(9) O'Dowd, C. D.; Jimenez, J. L.; Bahreini, R.; Plagan, R. C.; Seinfeld, J. H.; Hamerl, K.; Pirjola, L.; Kulmala, M.; Jennings, S. G.; Hoffmann, T. *Nature* **2002**, *417*, 632−636.
(10) Wayne, R. P. *Chemistry of Atmospheres*, 3rd ed.; Oxford University Press: Oxford, U.K., 2000.
(11) Fan, S. F.; Jacob, D. J. *Nature* **1992**, *359*, 522−524.
(12) Mozurkewich, M. *J. Geophys. Res., D: Atmos.* **1995**, *100* (7), 14199−14207.
(13) Vogt, R.; Crutzen, P. J.; Sander, S. *Nature* **1996**, *383*, 327−330.
(14) Sander, R.; Crutzen, P. J. *J. Geophys. Res., D: Atmos.* **1996**, *101* (4), 9121−9138.
(15) Oum, K. W.; Lakin, M. J.; DeHaan, D. O.; Brauers, T.; Finalyson-Pitts, B. J. *Science* **1998**, *279*, 74−77.
(16) McElroy, C. T.; McLinden, C. A.; McConnell, J. C. *Nature* **1999**, *397*, 338−341.
(17) Vogt, R.; Sander, R.; Glasow, R. V.; Crutzen, P. J. *J. Atmos. Chem.* **1999**, *32*, 375−395.
(18) Behnke, W.; Elend, M.; Krüger, U.; Zetzsch, C. *J. Atmos. Chem.* **1999**, *34*, 87−99.
(19) Knipping, E. M.; Lakin, M. J.; Foster, K. L.; Jungwirth, P.; Tobias, D. J.; Gerber, R. B.; Dabdub, D.; Finalyson-Pitts, B. J. *Science* **2000**, *288*, 301−306.
(20) Finalyson-Pitts, B. J.; Hemminger, J. C. *J. Phys. Chem. A* **2000**, *104*, 11463−11477.
(21) Foster, K. L.; Plastridge, R. A.; Bottenheim, J. W.; Shepson, P. B.; Finalyson-Pitts, B. J.; Spicer, C. W. *Science* **2001**, *291*, 471−474.
(22) Kawasaki, M.; Lee, S. J.; Bersohn, R. *J. Chem. Phys.* **1975**, *63*, 809−814.
(23) Schmitt, G.; Comes, F. J. *J. Photochem.* **1980**, *14*, 107−123.
(24) Kroger, P. M.; Demou, P. C.; Riley, S. J. *J. Chem. Phys.* **1976**, *65*, 1823−1834.
(25) Koffend, J. B.; Leone, S. R. *Chem. Phys. Lett.* **1981**, *81*, 136−141.
(26) Cain, S. R.; Hoffman, R.; Grant, R. *J. Phys. Chem.* **1981**, *85*, 4046−4051.
(27) Lee, S. J.; Bersohn, R. *J. Phys. Chem.* **1982**, *86*, 728−730.
(28) Butler, L. J.; Hintsa, E. J.; Lee, Y. T. *J. Chem. Phys.* **1986**, *84*, 4104−4106.
(29) Butler, L. J.; Hintsa, E. J.; Lee, Y. T. *J. Chem. Phys.* **1987**, *86*, 2051−2074.
(30) Wannenmacher, E. A. J.; Felder, P.; Huber, J. R. *J. Chem. Phys.* **1991**, *95*, 986−997.
(31) Baum, G.; Felder, P.; Huber, J. R. *J. Chem. Phys.* **1993**, *98*, 1999−2010.
(32) Marvet, U.; Dantus, M. *Chem. Phys. Lett.* **1996**, *256*, 57−62.
(33) Zhang, Q.; Marvet, U.; Dantus, M. *J. Chem. Phys.* **1998**, *109*, 4428−4442.
(34) Jung, K.-W.; Ahmadi, T. S.; El-Sayed, M. A. *Bull. Korean Chem. Soc.* **1997**, *18*, 1274−1280.
(35) Radloff, W.; Farmanara, P.; Stert, V.; Schreiber, E.; Huber, J. R. *Chem. Phys. Lett.* **1998**, *291*, 173−178.
(36) Kavita, K.; Das, P. K. *J. Chem. Phys.* **2000**, *112*, 8426−8431.
(37) Baughcum, S. L.; Hafmann, H.; Leone, S. R.; Nesbitt, D. *Faraday Discuss.* **1979**, *67*, 306−315.
(38) Baughcum, S. L.; Leone, S. R. *J. Chem. Phys.* **1980**, *72*, 6531−6545.
(39) Maier, G.; Reisenauer, H. P. *Angew. Chem., Int. Ed. Engl.* **1986**, *25*, 819−822.
(40) Maier, G.; Reisenauer, H. P.; Lu, J.; Schaad, L. J.; Hess, B. A., Jr. *J. Am. Chem. Soc.* **1990**, *112*, 5117−5122.
(41) Tarnovsky, A. N.; Alvarez, J.-L.; Yartsev, A. P.; Sündstrom, V.; Åkesson, E. *Chem. Phys. Lett.* **1999**, *312*, 121−130.
(42) Tarnovsky, A. N.; Wall, M.; Rasmusson, M.; Pascher, T.; Åkesson, E. *J. Chin. Chem. Soc.* **2000**, *47*, 769−772.
(43) Tarnovsky, A. N.; Wall, M.; Gustafsson, M.; Lascoux, N.; Sundström, V.; Åkesson, E. *J. Phys. Chem. A* **2002**, *106*, 5999−6005.
(44) Wall, M.; Tarnovsky, A. N.; Pascher, T.; Sundström, V.; Åkesson, E. *J. Phys. Chem. A* **2003**, *107*, 211−217.
(45) Zheng, X.; Phillips, D. L. *Chem. Phys. Lett.* **2000**, *324*, 175−182.
(46) Zheng, X.; Phillips, D. L. *J. Chem. Phys.* **2000**, *113*, 3194−3203.
(47) Zheng, X.; Phillips, D. L. *J. Phys. Chem. A* **2000**, *104*, 6880−6886.
(48) Zheng, X.; Kwok, W. M.; Phillips, D. L. *J. Phys. Chem. A* **2000**, *104*, 10464−10470.
(49) Zheng, X.; Fang, W.-H.; Phillips, D. L. *J. Chem. Phys.* **2000**, *113*, 10934−10946.
(50) Kwok, W. M.; Ma, C.; Parker, A. W.; Phillips, D.; Towrie, M.; Matousek, P.; Phillips, D. L. *J. Chem. Phys.* **2000**, *113*, 7471−7478.

(51) Zheng, X.; Lee, C. W.; Li, Y.-L.; Fang, W.-H.; Phillips, D. L. *J. Chem. Phys.* **2001**, *114*, 8347−8356.
(52) Kwok, W. M.; Ma, C.; Parker, A. W.; Phillips, D.; Towrie, M.; Matousek, P.; Zheng, X.; Phillips, D. L. *J. Chem. Phys.* **2001**, *114*, 7536−7543.
(53) Kwok, W. M.; Ma, C.; Parker, A. W.; Phillips, D.; Towrie, M.; Matousek, P.; Phillips, D. L. *Chem. Phys. Lett.* **2001**, *341*, 292−298.
(54) Li, Y.-L.; Wang, D.; Phillips, D. L. *Bull. Chem. Soc. Jpn.* **2002**, *75*, 943−948.
(55) Kwok, W. M.; Ma, C.; Parker, A. W.; Phillips, D.; Towrie, M.; Matousek, P.; Phillips, D. L. *J. Phys. Chem. A* **2003**, *107*, 2624−2628.
(56) Phillips, D. L.; Fang, W.-H.; Zheng, X. *J. Am. Chem. Soc.* **2001**, *123*, 4197−4203.
(57) Phillips, D. L.; Fang, W.-H. *J. Org. Chem.* **2001**, *66*, 5890−5896.
(58) Li, Y.-L.; Leung, K. H.; Phillips, D. L. *J. Phys. Chem. A* **2001**, *105*, 10621−10625.
(59) Fang, W.-H.; Phillips, D. L.; Wang, D.; Li, Y.-L. *J. Org. Chem.* **2002**, *67*, 154−160.
(60) Li, Y.-L.; Chen, D. M.; Wang, D.; Phillips, D. L. *J. Org. Chem.* **2002**, *67*, 4228−4235.
(61) Li, Y.-L.; Wang, D.; Phillips, D. L. *J. Chem. Phys.* **2002**, *117*, 7931−7941.
(62) Tarnovsky, A. N.; Sundstrom, V.; Akesson, E.; Pascher, T. *J. Phys. Chem. A* **2004**, *108*, 237−249.
(63) Harding, L. B.; Schlegel, H. B.; Krishnan, R.; Pople, J. A. *J. Phys. Chem.* **1980**, *84*, 3394−3401.
(64) Pople, J. A.; Raghavachari, K.; Frisch, M. J.; Blinkley, J. B.; Schleyer, P. V. R. *J. Am. Chem. Soc.* **1983**, *105*, 6389−6398.
(65) Wesdemiotis, C.; Feng, R.; Danis, P. O.; Williams, E. R.; Lafferty, F. W. *J. Am. Chem. Soc.* **1986**, *108*, 5847−5853.
(66) Yates, B. F.; Bouma, W. J.; Radom, L. *J. Am. Chem. Soc.* **1987**, *109*, 2250−2263.
(67) Kirmse, W.; Meinert, T.; Moderelli, D. A.; Platz, M. S. *J. Am. Chem. Soc.* **1993**, *115*, 8918−8927.
(68) Walch, S. P. *J. Chem. Phys.* **1993**, *98*, 3163−3178.
(69) Gonzalez, C.; Restrepo-Cossio, A.; Márquez, M.; Wiberg, K. B. *J. Am. Chem. Soc.* **1996**, *118*, 5408−5411.
(70) Moody, C. J.; Whitman, G. H. In Reactive Intermediates; Davies, S. G., Ed.; Oxford University Press: New York, 1992.
(71) Pliego, J. R., Jr.; De Almeida, W. B. *J. Phys. Chem.* **1996**, *100*, 12410−12413.
(72) Pliegeo, J. R., Jr.; De Almeida, W. B. *J. Phys. Chem. A* **1999**, *103*, 3904−3909.
(73) Kwok, W. M.; Zhao, C.; Li, Y. L.; Guan, X.; Phillips, D. L. *J. Chem. Phys.* **2004**, *120*, 3323−3332.
(74) Kwok, W. M.; Zhao, C.; Li, Y. L.; Guan, X.; Wang, D.; Phillips, D. L. *J. Am. Chem. Soc.* **2004**, *126*, 3119−3131.
(75) Kwok, W. M.; Zhao, C.; Guan, X.; Li, Y. L.; Du, Y.; Phillips, D. L. *J. Chem. Phys.* **2004**, *120*, 9017−9032.
(76) Frisch, M. J.; Trucks, G. W.; Schlegel, H. B.; Scuseria, G. E.; Robb, M. A.; Cheeseman, J. R.; Zakrzewski, V. G.; Montgomery, J. A., Jr.; Stratmann, R. E.; Burant, J. C.; Dapprich, S.; Millam, J. M.; Daniels, A. D.; Kudin, K. N.; Strain, M. C.; Farkas, O.; Tomasi, J.; Barone, V.; Cossi, M.; Cammi, R.; Mennucci, B.; Pomelli, C.; Adamo, C.; Clifford, S.; Ochterski, J.; Petersson, G. A.; Ayala, P. Y.; Cui, Q.; Morokuma, K.; Malick, D. K.; Rabuck, A. D.; Raghavachari, K.; Foresman, J. B.; Cioslowski, J.; Ortiz, J. V.; Stefanov, B. B.; Liu, G.; Liashenko, A.; Piskorz, P.; Komaromi, I.; Gomperts, R.; Martin, R. L.; Fox, D. J.; Keith, T.; Al-Laham, M. A.; Peng, C. Y.; Nanayakkara, A.; Gonzalez, C.; Challacombe, M.; Gill, P. M. W.; Johnson, B. G.; Chen, W.; Wong, M. W.; Andres, J. L.; Head-Gordon, M.; Replogle, E. S.; Pople, J. A. *Gaussian 98*, revision A.7; Gaussian, Inc.: Pittsburgh, PA, 1998.
(77) Gonzalez, C.; Schlegel, H. B. *J. Chem. Phys*. **1989**, *90*, 2154−2161.
(78) Gonzalez, C.; Schlegel, H. B. *J. Phys. Chem.* **1990**, *94*, 5523−5527.
(79) Achatz, U.; Fox, B. S.; Beyer, M. K.; Bondybey, V. E. *J. Am. Chem. Soc.* **2001**, *123*, 6151−6156.
(80) Lee, H. M.; Kim, K. S. *J. Chem. Phys.* **2001**, *114*, 4461−4471.
(81) Kowal, M.; Gora, R. W.; Roszak, S.; Leszczynski, J. *J. Chem. Phys.* **2001**, *115*, 9260−9265
(82) Conley, C.; Tao, F. M. *Chem. Phys. Lett.* **1999**, *301*, 29−36.
(83) Gertner, B. J.; Peslherbe, G. H.; Hynes, J. T. *Isr. J. Chem.* **1999**, *39*, 273−281.
(84) Milet, A.; Struniewicz, C.; Moszynski, R.; Wormer, P. E. S. *J. Chem. Phys.* **2001**, *115*, 349−356.
(85) Cabaleiro-Lago, E. M.; Hermida-Ramón, J. M.; Rodríguez-Otero, J. *J. Chem. Phys.* **2002**, *117*, 3160−3168.
(86) Hurley, S. M.; Dermota, T. E.; Hydutsky, D. P.; Castleman, A. W., Jr. *Science* **2002**, *298*, 202−204.
(87) Voegele, A. F.; Liedl, K. R. *Angew. Chem., Int. Ed.* **2003**, *42*, 2114−2116.
(88) Knuttu, H.; Dahlqvist, M.; Murto, J.; Räsänen, M. *J. Phys. Chem.* **1988**, *92*, 1495−1502.
(89) Tyndall, G. S.; Wallington, T. J.; Hurley, M. D.; Schneider, W. F. *J. Phys. Chem.* **1993**, *97*, 1576−1582.
(90) Wallington, T. J.; Schneider, W. F.; Barnes, I.; Becker, K. H.; Sehested, J.; Nielsen, O. J. *Chem. Phys. Lett.* **2000**, *322*, 97−102.
(91) Le Botlan, D. J.; Mechin, B. J.; Martin, G. J. *Anal. Chem.* **1983**, *55*, 587−591.
(92) Bell, R. P. *Adv. Phys. Org. Chem.* **1966**, *4*, 1−27.
(93) Zavitsas, A. A.; Coffiner, M.; Wiseman, T.; Zavitsas, L. R. *J. Phys. Chem.* **1970**, *74*, 2746−2750.
(94) Wolfe, S.; Kim, C. K.; Yang, K.; Weinberg, N.; Shi, Z. *J. Am. Chem. Soc.* **1995**, *117*, 4240−4260.
(95) Guan, X.; Du, Y.; Li, Y.-L.; Kwok, W. M.; Phillips, D. L. *J. Chem. Phys.* **2004**, *121*, 8399−8409.